UNITED STATES DEPARTMENT OF THE INTERIOR

GEOLOGICAL SURVEY

Test and Calibration of the Seismic Research Observatory

by

Jon Peterson,

Charles R. Hutt,

L. Gary Holcomb

Open-File Report 80-187

Albuquerque, New Mexico

1980

CONTENTS

Page

1.0 INTRODUCTION 1

2.0 SRO SYSTEM DESCRIPTION 4

3.0 THE SRO TESTING PROGRAM 9

4.0 ERRORS ASSOCIATED WITH SRO ANALOG-TO-DIGITAL CONVERSION 14

4.1 General

4.2 Aliasing

4.3 Quantizing Error

4.4 ADC Tracking Error, Aperture Error, Jitter Error, Nonlinearities, and Noise

4.5 Apparent Peak-to-Peak Amplitude Errors

5.0 STEADY-STATE CALIBRATION 23

5.1 General

5.2 SRO Calibration Circuit

5.3 SRO Displacement Sensitivity

5.4 Frequency Response Measurements

6.0 SRO SYSTEM NOISE TESTS 39

6.1 Seismometer Noise Tests

6.2 Recording System Noise Tests

7.0 NON-LINEAR DISTORTION 52

7.1 Clipping Thresholds

7.2 Intermodulation Distortion

8.0 SEISMOMETER ORIENTATION AND POLARITY 60

9.0 SRO SYSTEM TRANSFER FUNCTIONS 62

9.1 General

9.2 Seismometer

9.3 Seismic Filters

9.4 Anti-Aliasing Filters

9.5 Nominal System Transfer Functions

9.6 SRO Component Transfer Functions

ACKNOWLEDGEMENT 84

REFERENCES 85

1.0 INTRODUCTION

The Seismic Research Observatory (SRO) network is generating an important new data base for seismological research. The SRO systems have extended both the range and resolution of seismic measurements beyond the limits of conventional seismographs and the data are recorded in digital format making it convenient to automate processing and analysis. The SRO network now comprises 12 stations (see Figure 1.1) and one additional station will be installed. The data produced by the SRO network, and other digital systems being installed to supplement the SRO network, will be collected by the U.S. Geological Survey's Albuquerque Seismological Laboratory, organized into network-day tapes, and made available to research organizations throughout the world. The network-day tapes are particularly unique and useful data files as they will contain not only seismic data but all of the information needed by an analyst to interpret the data, including station constants and calibration and other instrumental parameters. Hoffman (in preparation) describes these tapes and the format used in their compilation.

The global digital data base for seismology is still relatively limited in terms of both geographical and temporal coverage. For this reason there is a tendency, perhaps, to stretch the applicability of the available data beyond the intended purposes. The danger in this is compounded by the fact that computer processing and analysis often can be done without even looking at the waveforms, and it is done with deceptively high computational precision that belies the basic accuracy of the measurements. The day may be passing when seismologists have a hands-on familiarity with the data acquisition

systems, but clearly it is as important as ever that they have a knowledge of the capabilities and limitations of the instruments.

The primary objective of the SRO network was to lower the threshold of event detection in the long-period band. This was achieved by using a newly-developed borehole seismometer that is capable of resolving both vertical and horizontal components of earth background noise at the quietest sites on earth. Another objective was to accommodate a large range of signal amplitudes. This was achieved by using an advanced digital recording system which provides at least 110 dB of separation between system noise levels and clipping levels in the principal bands of interest. The broadband capability of the SRO system has been demonstrated. This capability was not an initial program requirement and is not being fully utilized at present, but it adds significantly to the research potential of the network. The SRO systems have proven to be reliable in operation and the general quality of the data is excellent.

Every seismograph has functional limits and limits of accuracy, and the SRO system is no exception. The chief purpose of this report is to define these limits for the SRO system and provide the most accurate calibration data currently available. At the same time we will describe the testing program in sufficient detail so that the data user can make his own judgments regarding the effectiveness and accuracy of the tests. This report is not a final statement; further work is needed in some areas to completely define the SRO system, in some cases purely for academic reasons. Refinements in calibration will appear on the network-day tapes as the new data become available.

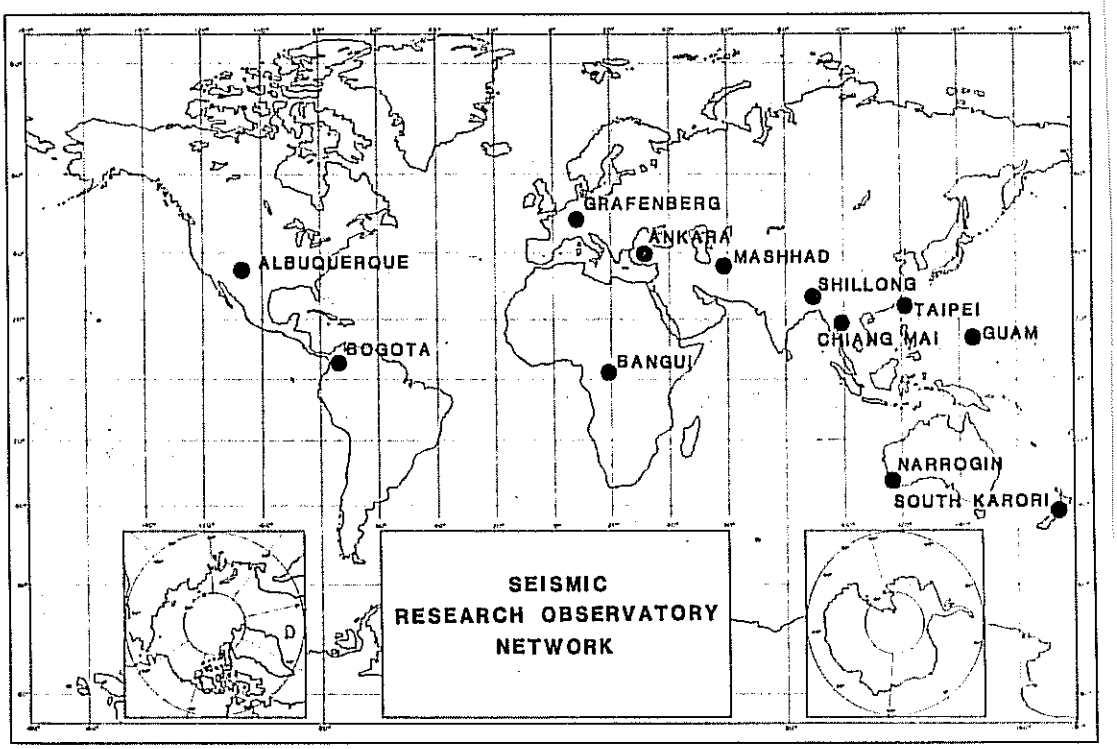

Figure 1.1.--The Seismic Research Observatory Network. For installation dates, see Table 2.1. One additional station will be installed.

2.0 SRO SYSTEM DESCRIPTION

The Seismic Research Observatory has been described by Peterson and others (1976). A far more technical description of the instrumentation will be found in the operation and maintenance manuals. A complete description of the KS 36000 seismometer and associated components is given in manuals published by Teledyne-Geotech (1976a-1976i) and the SRO recording system is described in a manual published by Unitech Inc. (1974). The following brief summary is intended to serve only as background information for this report.

The Seismic Research Observatory system consists of a borehole seismometer, an advanced recording system that produces both analog and digital records, and associated equipment needed for timing, power, and control (see Figure 2.1). The seismometer system has two major parts: a downhole package that contains the set of three orthogonal sensors plus electronics, and an uphole package, called the wellhead terminal, that contains seismic filters, a control panel, and calibration equipment. The downhole package is designed for installation in standard 7-inch well casing and it is normally installed at a depth of about 100 meters.

The sensors are force-balance accelerometers designed to have a closed-loop period of 1 second and a closed-loop damping of 80% of critical. The fundamental output of each sensor, called the mass position output, is proportional to earth acceleration from 0 to about 1 Hz and has a nominal sensitivity of 1,000 volts/meter/second^2. Normally, the mass position output is not recorded although it can be monitored (one component at a time) on the auxiliary channel. The mass position signal from each sensor is passed

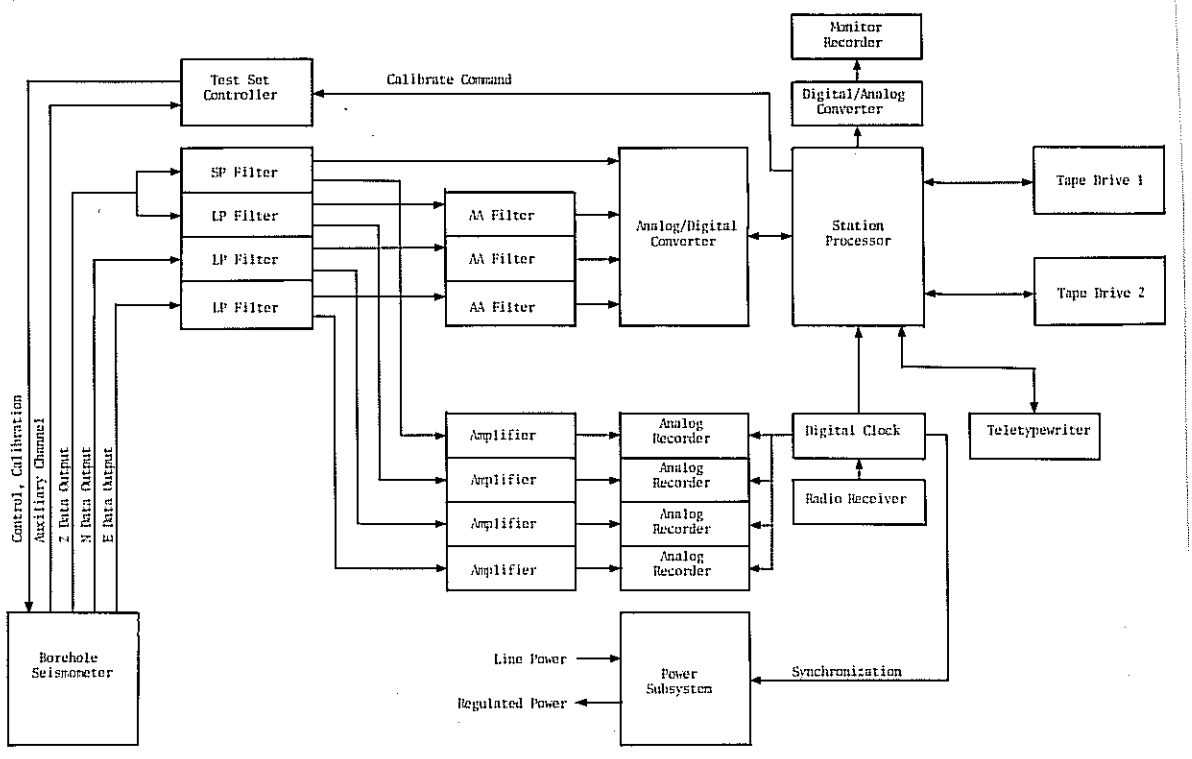

Figure 2.1.--Block diagram of the SRO system showing major components.

through a band-pass circuit having design corner frequencies of .02 and 16 Hz and a gain of 46 dB. This signal, called the data output, is transmitted uphole by a line driver having an additional gain of 20 dB and a low-pass section cornered at 42 Hz. The downhole circuits are described in more detail in Section 9.0. In the wellhead terminal the data output signal is further shaped by seismic filters to produce a conventional long-period output peaking at about 28 seconds period and, in the case of the vertical component, a short-period output peaking at about 0.4 seconds.

The seismic filters have parallel outputs. One is used for analog recording and the other is used for digital recording. Analog seismograms are produced on visual drum recorders using heat-sensitive paper as the recording

medium. The long-period signals are passed through anti-aliasing filters prior to digitization. Originally, these were 4-pole Butterworth filters but they have been replaced with 4-pole Bessel filters, which have improved noise, offset, and phase response characteristics. Short-period anti-aliasing filters were furnished with the SRO systems but these were removed before any stations became operational. Some of the stations had single-pole low-pass sections cornered at 16 Hz in the short-period channels. These too have been removed.

The digital-recording system consists of a gain-ranged analog-to-digital converter, a station processor with 8 kilobytes of memory (now being increased to 16 kilobytes of memory), and magnetic tape recorders. The analog-to-digital converter samples the long-period signals once each second and the short-period signal 20 times each second. As each sample is taken, an 11-step binary-gain amplifier scales it to within 6 dB of the full-scale input to the analog-to-digital converter. Four bits specifying the amplifier gain are prefixed to the 12 data bits generated by the converter to form a 16-bit word which is recorded on tape. Long-period data are recorded continuously on tape; however, only events as detected by the station processor in the short-period signal are recorded in order to conserve tape and reduce the volume of data generated by the network. Two tape drives are furnished with each system to maintain uninterrupted recording. Normally, tapes are changed at two-week intervals.

The station operator communicates with the station processor and controls the SRO system using a Teletypewriter. The operating software permits him to select recording modes, adjust gain levels, set event detection parameters, calibrate the sensors (routine daily calibration is automated), and perform other functions. Short-period event on-and-off times are automatically printed on the station log. Copies of the Teletype-

writer log are sent in with the data tapes and kept on file at the Albuquerque Seismological Laboratory.

At six of the SRO stations the borehole seismometers are located at remote sites some distance from the recording systems and telemetry links are used to transmit commands and signals between the seismometer site and the recording station site. Radio links are used at two of these stations, telephone circuits at three, and hardwire at one. In the telemetry mode, the seismic signals are digitized at the remote site and transmitted in digital form. At the recording system end of the link digital-to-analog converters are used to produce the analog signals for visual recording. There are no differences in the recording format or data response characteristics; however, data users may notice occasional dropouts caused by transmission interruptions.

At three of the SRO stations (Guam, South Karori, Taipei) the short-period earth noise levels are very high because of proximity to the coast. At these stations the vertical-component mass position signal is brought uphole on the auxiliary channel and used in place of the data output signal to drive the short-period filters. This reduces the sensitivity of the short-period signal by 60 dB.

The operational configurations of the SRO stations are given in Table 2.1, and the Table provides a history of the changes that have been made.

Station	Code	Open	Telemetry Circuit	LP Anti-Aliasing Filter		Low-Pass Section	Special Low-Gain Short Period
				Butterworth	Bessel		
Albuquerque, New Mexico	ANMO	08/74	none	08/74-12/75	12/75-	08/74-10/78	no
Ankara, Turkey	ANTO	08/78	hardwire	no	08/78-	no	no
Bangui, Central African Republic	BCAO	06/79	none	no	06/79-	no	no
Bogota, Columbia	BOCO	12/77	radio	no	12/77-	no	no
Chiang Mai, Thailand	CHTO	06/77	none	06/77-07/79	07/79-	06/77-02/79	no
Grafenberg, Germany	GRFO	10/78	telephone	no	10/78-	10/78-06/79	no
Guam, Mariana Islands	GUMO	07/75	none	07/75-12/79	12/79-	no	yes
Mashhad, Iran	MAIO	10/75	none	10/75-	no	no	no
Narrogin, Australia	NWAO	04/76	telephone	04/76-01/79	01/79-	04/76-11/77	no
Shillong, India	SHIO	06/78	none	no	06/78-	no	no
South Karori, New Zealand	SNZO	03/76	telephone	03/76-11/78	11/78-	03/76-10/78	yes
Taipei, Taiwan	TATO	05/76	radio	05/76-01/79	01/79-	05/76-12/78	yes

Table 2.1.--Operating configuration of SRO stations.

3.0 THE SRO TESTING PROGRAM

The Seismic Research Observatory is one of the most thoroughly tested and documented seismograph systems in existence. One reason for this is that the SRO concept, especially for the seismometer, required significant departures from conventional design. A comprehensive test plan was designed by the manufacturer and project personnel to verify that the design objectives have been met. Later this plan was modified and expanded for use in acceptance of the production equipment and for testing the operational systems during installation and maintenance.

A partial list of tests performed on the SRO systems at various stages in the program is given in Table 3.1. Only those that have a bearing on data accuracy and quality are shown; not listed are functional measurements such as diagnostic procedures used for fault isolation. All of the results of the measurements are documented. The documentation, which includes analog and digital records, is on permanent file at the Albuquerque Seismological Laboratory.

The factory tests are intended principally for the purpose of insuring that the instruments operate within prescribed tolerances. One of the more important of these procedures is the measurement of noise generated within the loop boards located in the downhole electronics package. Since the sensor mass cannot be blocked for noise tests, the manufacturer developed a special device that simulates the low signal levels in the feedback loop of an operating sensor. The simulation has been very effective in isolating marginal electronic components. Several of the factory measurements are critical to the accuracy of calibration and these are described in Section 5.0.

FACTORY	ALBUQUERQUE SEISMOLOGICAL LABORATORY	INSTALLATION	ROUTINE STATION TESTS
Modules	Routine Check-Out Procedures	Routine Check-Out Procedures	LP Calibration
Determination of Feedback Coil Motor Constant "G"	Data Output Sensitivity	Data Output Sensitivity	SP Calibration
Open-Loop Period Range	Mass Position Readings	Mass Position Readings	Time Error
Open-Loop Damping Range	Polarity Settings	Polarity Settings	
Transducer Sensitivity Range	Seismometer Clipping Level	Seismometer Clipping Level	DATA REVIEW
Electronic Subassembly	Calibration Signal Levels	Calibration Signal Levels	Data Quality Check
Noise (Simulator Test)	Auxiliary Line Driver Gain	Auxiliary Line Driver Gain	Calibration
Distortion	LP Filter Amplitude Response	LP Filter Amplitude Response	Error Checks
LP Filters	LP Filter Distortion	LP Filter Distortion	
Gain	SP Filter Amplitude Response	SP Filter Amplitude Response	SCHEDULED MAINTENANCE
Common Mode Rejection	SP and LP Filter Noise Tests	SP and LP Filter Noise Tests	Calibration Signal Levels
DC Offset	SP and LP Filter Offset Adjustments	SP and LP Filter Offset Adjustments	Auxiliary Line Driver Gain
Distortion	System SP Amplitude Response	System SP Amplitude Response	SP and LP Filter Noise Tests
Noise	System LP Amplitude Response	System LP Amplitude Response	System SP Amplitude Response
SP Filters	System Distortion	System Distortion	System LP Amplitude Response
Gain	Comparison with Standard SRO	Recording System Noise Test	Recording System Noise Tests
Common Mode Rejection		Digital Sensitivity	Digital Sensitivity
DC Offset		Analog Magnification	Analog Magnification
Noise			Polarity Settings
Seismometer			
Analog Calibration Levels			SPECIAL CALIBRATION TESTS
Digital Calibration Levels			Data Output Amplitude and Phase
Auxiliary Line Driver Gain			SP Filter Amplitude and Phase
Data Output Sensitivity			LP Filter Amplitude and Phase
SP System Amplitude Response			AA Filter Amplitude and Phase
SP System Sensitivity			System SP Amplitude and Phase
LP System Amplitude Response			System LP Amplitude and Phase
LP System Distortion			
LP System Sensitivity			
Borehole Operation			

Table 3.1.--Partial list of documented tests on SRO systems.

Many of the factory tests were repeated at the Albuquerque Seismological Laboratory as part of the acceptance procedures, but the paramount consideration during this phase of testing was the evaluation of instrument noise. At Albuquerque the seismometers were operated for the first time in a seismically quiet environment and for the first time were connected to the SRO recording systems. After routine tests were completed each seismometer was operated for a period of at least one week in a borehole adjacent to the ANMO seismometer which has served as a standard for comparison and tests throughout the program.

During the field installation of an SRO system performance checks are repeated to insure that the instruments were not damaged in transit. Then measurements are made to determine the recording system noise levels (which can vary as a function of local grounding techniques), determine frequency response characteristics, and determine distortion levels in the final operating configuration. The sensitivity levels are adjusted and there are special procedures for establishing proper polarity and orientation. The results of these measurements and tests are documented in the Station Installation Reports.

When a station is functioning normally, few operator-initiated tests are necessary. Periodic sine-wave calibration of the sensors is automated. With respect to data quality the most important function of the station operator is the daily time check. Using radio-transmitted timing signals the operator measures the clock error and records the correction on the teletype log and the seismograms. In the future, the clock corrections will also be recorded in the headers of the digital records. The clock error is reset to zero at each tape change or whenever the error exceeds 50 milliseconds.

Data tapes and seismograms are carefully reviewed as they pass through the Albuquerque Seismological Laboratory. The review includes the analysis of a graphic display of seismic background levels and calibration signals. Hard copies of the display are filed with the logs. The tapes are then run through an edit program that lists timing errors, data dropouts, record length errors, parity errors, and so forth. Where possible, these errors are corrected as the tapes are copied. Statistical tapes containing calibration signals and various event detection parameters, including long-term averages of earth noise, are compiled from the station tapes during copying. The statistical tapes are a convenient source of data for in-house evaluation of the stability and proper setting of various system parameters.

Maintenance visits by project technicians are scheduled to each station, usually once or twice a year. These visits are intended primarily to maintain calibration, instrument noise levels, and other parameters within prescribed tolerances. They also provide the opportunity to update the SRO systems with hardware and software modifications. Work performed during the visits is documented in Station Maintenance Reports.

Special calibration measurement techniques have been developed that permit greater accuracy in calibration. In time, these measurements will be made at each station and repeated at intervals of perhaps a year. The tests, which are described in Section 5.0, require special equipment that must be transported from station to station. The results of these measurements are the basis for developing individual transfer functions for each seismometer component in the network.

Finally, in addition to the routine tests, there is a continuing program of SRO test and evaluation using both the ANMO station and other equipment available at Albuquerque. Hardware changes, software changes,

and new test procedures are all thoroughly evaluated before they are implemented on a network-wide basis.

4.0 ERRORS ASSOCIATED WITH SRO ANALOG-TO-DIGITAL CONVERSION

4.1 General

When using SRO digital data, or any digital data, an analyst must consider certain limitations and possible errors inherent in the analog-to-digital conversion process. Among these limitations and possible errors are aliasing, quantizing error, tracking error, sampling window (aperture error), jitter error, nonlinearities, and apparent peak-to-peak amplitude errors. These are discussed briefly in the following paragraphs as they relate to the SRO system.

4.2 Aliasing

The analog signals generated by the SRO seismic sensor system are digitized at discrete intervals and recorded on tape. The relationship of the sampling rate to the highest frequency contained in the analog data is important. The SRO system samples the short-period signal 20 times each second (20 Hz) and the long-period signals once each second (1 Hz). The Nyquist frequency is defined as one half of the sampling frequency; 10 Hz for the SRO short-period channels and 1/2 Hz for the long-period channels.

The sampling theorem states that, in order to be able to reconstruct the original analog signal with complete fidelity, it must be sampled at a rate greater than twice its highest frequency (see, for example, Stearns, 1975). If the signal is sampled too slowly so that it contains frequencies equal to or higher than the Nyquist frequency, a phenomenon known as aliasing will occur. As an example of aliasing assume that a sine wave whose frequency

f_a is 2/3 Hz is sampled at a frequency of 1 Hz. The result is illustrated in Figure 4.1. Note that the digital output is the same for input frequencies

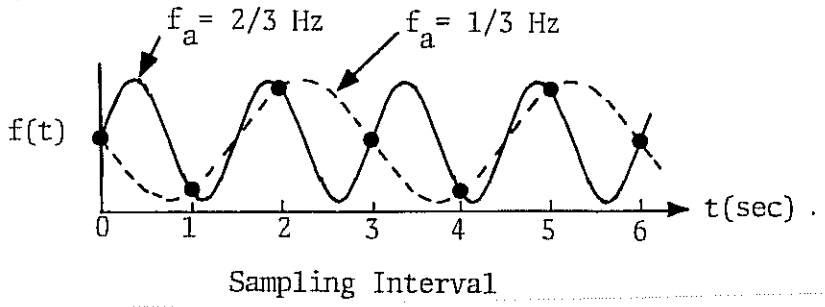

Figure 4.1.--Aliasing. (Adapted from Stearns, 1975.)

of either 1/3 or 2/3 Hz. The lower frequency would appear in a reconstructed analog signal or in a spectral representation of the digital signal. The true frequency, 2/3 Hz, is "folded" about the Nyquist frequency as illustrated in Figure 4.2 to produce an apparent or "aliased" signal with a frequency

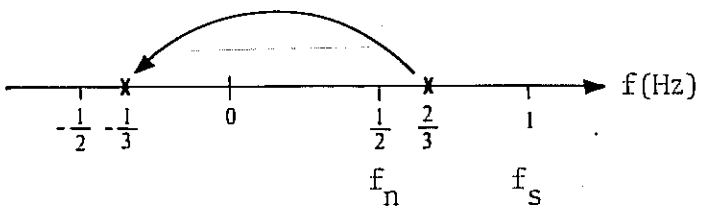

Figure 4.2.--Folding about the Nyquist frequency. (Adapted from Stearns, 1975.)

of 1/3 Hz. Figure 4.2 is not general. A more general form of the specific example cited can be stated as follows: Given a sampling frequency of f_s Hz, frequency components at f_a and $f_a + nf_a$ Hz are indistinguishable when digitized, n being any integer (Stearns, 1975).

Aliasing of the data can be prevented by low-pass filtering of the analog signal to eliminate energy at frequencies higher than the

Nyquist frequency. If the noise and signal spectra at the filter input were flat, the amount of filtering needed at the Nyquist frequency would be equal to the resolution of the recording system, 66 dB in the case of the SRO system. This requirement is offset to some extent in the seismic short-period band by the fact that earth displacements generated by signals and noise decrease with increasing frequency (see, for example, Hanks and Wyss, 1972, and Brune and Oliver, 1959). In the long-period band, however, more than 66 dB of filtering is needed because of noise and high signal levels in the band just above the Nyquist frequency.

Originally, anti-aliasing filters were used in both short- and long-period channels of the SRO system. The short-period anti-aliasing filters proved to be excessively noisy and were removed before any of the SRO stations became operational. They have not been replaced, because the combination of earth noise decay at higher frequencies and reduced seismometer sensitivity at short-periods provides inherent anti-alias filtering.

4.3 Quantizing Error

The SRO analog-to-digital converter (ADC) uses a 12-bit (11 bits plus sign) digitizer driven by an eleven-step binary gain amplifier (BGA). The amplifier has gain steps from 2^0 to 2^{10} (1 to 1,024). The full-scale value of the digitizer corresponds to 10.24 volts, so that one least-significant bit (LSB) is equivalent to $10.24 \div 2^{11}$ or 5 millivolts at the input to the digitizer (or the output of the BGA). If the BGA gain is 2^0, then one LSB corresponds to 5 millivolts at the BGA input. However, if the input signal is small and the BGA gain is set to 2^{10}, then one LSB corresponds to 5 millivolts $\div 2^{10}$ or 4.88 microvolts. One digital count is defined as one LSB for a BGA gain of 2^{10}, or 4.88 microvolts. Therefore, when the BGA gain is 2^0, a change of one LSB corresponds to 1,024 digital counts, or

5 millivolts.

If the BGA gain is fixed at 1 (2^0), and the input signal from the seismic system is 5.000 volts, the corresponding output is 1,024,000 digital counts. If the input signal increases to 5.001 volts the ADC output will remain fixed at 1,024,000 counts because the input signal has not increased enough to cause the digitizer to jump to the next quantization level. In fact, it will not do so until the input signal increases above 5.0025 volts, or more than half way to 5.005 volts, the next quantization level. The ADC output will then jump to 1,025,024 counts.

Such discrepancies between the analog input level and digital output representation are known as quantizing errors, the magnitude of which depend solely upon the resolution of the system. Since the SRO system has eleven-bit resolution, the maximum quantization error is one half of $1/2^{11}$, or .024%. This is true for all gain settings of the BGA, since the BGA gain has no effect on relative resolution.

4.4 ADC Tracking Error, Aperture Error, Jitter Error, Nonlinearities, and Noise

Tracking error is significant only when the input signal contains high frequencies that require a very high sampling rate. It is caused by the fact that the ADC has an input series resistance and shunt capacitance, and therefore requires some finite time to settle to the value present on the channel currently selected by the multiplexer. In the SRO system the ADC is relatively slow, having a maximum throughput rate of 1 KHz when used in the standard SRO mode of automatic gain ranging and multiplexed input. However, the input data contains very low frequencies when compared to this throughput rate. Therefore tracking error is negligible in the SRO system.

Aperture error arises when the sampling window is relatively wide compared to the input frequency. The SRO ADC has an aperture time of 50 nanoseconds, so it can be considered an impulse sampler with essentially zero aperture error, considering that the highest input frequency is about 5 Hz on the short-period channel.

Jitter error occurs when the sampling period varies randomly, producing errors equivalent to quantizing errors. The magnitude of jitter error is not precisely known for the SRO system, but is thought to be of the same order as the quantizing error discussed in Section 4.3, and is therefore negligible. Another type of timing error that is present in the SRO system is caused by the sequential multiplexing, conversion time, and delay in appending the header time to the data records. The SP channel is sampled, say, at zero time, then the LPZ channel is sampled 1.1 milliseconds later, followed by the LPN and LPE channels at 1.1 millisecond intervals. Then the SP channel is sampled every 50 milliseconds until 20 SP samples have been taken, at which time the one second sequence (frame) repeats. The clock time is read by the computer as soon as the beginning of each frame causes an interrupt, so that the header time associated with the first SP data sample is a few microseconds later than the real sample time. In the telemetered systems, the header time can be as much as 3 to 4 milliseconds later than the first SP sample time, because of delays in the telemetry links. None of these timing errors are considered significant, because they are small compared to the sampling interval and because the smallest interval of time resolved by the header is 10 milliseconds.

ADC nonlinearities are produced by a range of possible problems. These include bit dropouts, non-uniform quantization level spacing, zero discontinuity, and BGA gain errors. Bit dropouts are almost non-existent in the SRO ADC. Non-uniform quantization level spacing is also small enough

to be negligible, as determined by tests performed at the Albuquerque Seismological Laboratory. Zero discontinuity and BGA gain errors (which can produce discontinuities at levels other than zero) can be significant if the ADC is not adjusted properly or has some electronic problems. The SRO ADCs are checked routinely and repaired or adjusted if any of these problems appear. These latter four possible problems are discussed at greater length in the ADC Operation and Maintenance Manual (Phoenix Data, 1973).

ADC noise in the SRO system is 2 to 4 digital counts when the BGA gain is 2^{10}, and 1 to 2 LSBs when the BGA gain is lower than 2^{10}.

A more theoretical and detailed discussion of most of the possible errors discussed in this Section can be found in Stearns (1975), Otnes and Enochson (1972), Bendat and Piersol (1971), and Phoenix Data (1973).

4.5 Apparent Peak-to-Peak Amplitude Errors

Most digital recording systems use a digitizer running at a fixed rate for each channel of input data, although the sampling rates may vary from one channel to the next. The SRO recording system is no different in this respect. Since the SRO digitizer has 11-bit resolution, the recorded digital data are usually assumed to have a basic accuracy of 1 part in 2^{11}, or about .05%. However, when the sinusoidal frequencies present in the analog input signals approach one-twentieth of the sample frequency, peak-to-peak amplitude errors in the digitized values can be as large as 1%, even if the digitizer itself is perfect. Input signal frequencies that approach the Nyquist frequency are subject to errors as large as 100%.

The reason for these errors can best be demonstrated by an example. Suppose the digitizer sample frequency f_s is 1 Hz, and the analog input signal is a sine wave whose frequency f_a is .25 Hz (4 seconds period). If

the phase relationship between the digitizer clock and the input signal is such that a sample is taken at the zero-crossing of the input signal, then the next sample will be at a peak, the next at a zero-crossing, the next at the opposite peak, and so on. In this case the recorded peak-to-peak amplitude is maximum and is equal to 1.00 times the actual peak-to-peak amplitude of the signal. However, if the digitizer clock is out of phase with the input signal by 45 degrees, the recorded peak-to-peak amplitude would be .707 times the actual peak-to-peak amplitude of the input signal. This would be the worst-case condition for f_a = .25 Hz, and represents the minimum possible recorded p-p amplitude for this particular frequency. The phase relationship between the digitizer and the input signal is random for random input signals. Therefore, for f_a =.25 Hz and f_s = 1.00 Hz, the recorded p-p amplitude can be anywhere between 100% and 70.7% of the actual input amplitude.

Figure 4.3 shows a plot of maximum and minimum possible recorded p-p amplitudes as a function of input frequency. The Nyquist frequency is indicated on the plot, as are the 2%, 5%, and 10% error limits. The 5% error limit for the SRO short-period data is 2.4 Hz. This means that all recorded p-p amplitudes that are caused by input signal frequencies of 2.4 Hz or less will be in error by no more than 5%. Note that the error is always zero or negative; that is, the recorded p-p amplitude is always less than or equal to the true input p-p amplitude.

The peaks in the maximum curve and the troughs in the minimum curve occur at the points where there are an even number of samples per cycle. The troughs in the maximum curve occur at the points where there are an odd number of samples per cycle.

The sampling theorem guarantees that, for input frequencies less than 1/2 f_s, we can always perfectly reconstruct the analog data from

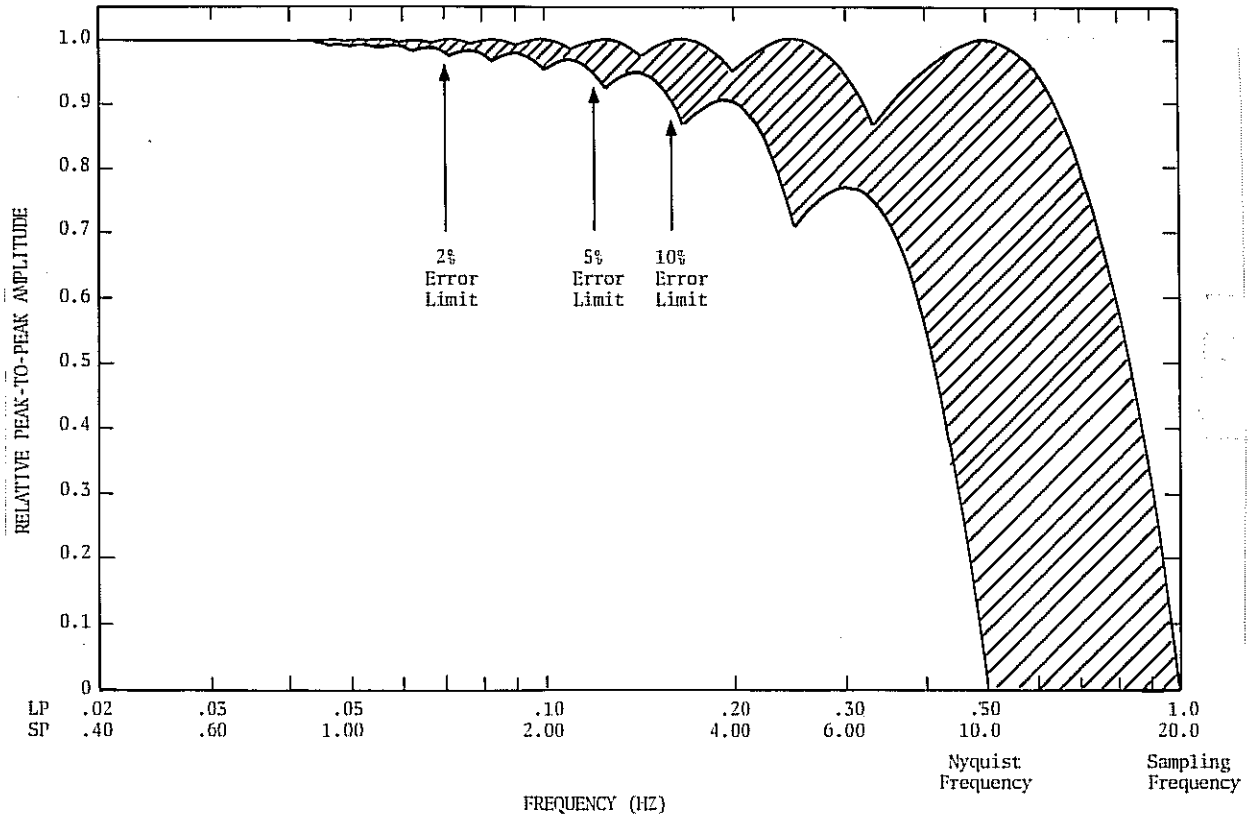

Figure 4.3.--Digital system frequency response. The shaded area represents the possible range of digital peak-to-peak amplitudes recorded when a sine wave of frequency f is applied to the input of a digital recording system whose digitizer is running at sample frequency f_s.

the recorded digital data. However, this type of reconstruction is rarely done in the routine analysis of seismic data. If the analyst plots a waveform from the SRO digital data, he usually does so by plotting the points on a graphic display device and connecting the points together with straight lines. Waveforms obtained by this technique are, of course, subject to the p-p amplitude errors discussed here. (Note that the SRO analog seismograms from telemetered sites are also subject to the same errors, since they are produced from telemetered digital data.) Table 4.1 lists the 2%, 5%, and 10% error limit frequencies and periods for both the

SRO short-period and long-period data. The analyst should keep these limits and Figure 4.3 in mind when using waveforms plotted from the digital data.

	2% Error limit		5% Error limit		10% Error limit	
	f(Hz)	T(sec)	f(Hz)	T(sec)	f(Hz)	T(sec)
LP (f_s = 1.00 Hz)	.070	14.3	.12	8.33	.16	6.25
SP (f_s = 20.0 Hz)	1.4	.714	2.4	.417	3.2	.313

Table 4.1.--Error limit frequencies for SRO LP and SP digital data.

5.0 STEADY-STATE CALIBRATION

5.1 General

The purpose of seismograph calibration is to provide a relationship between the input function -- usually expressed in units of earth displacement, velocity, or acceleration -- and the signals recorded by the seismograph. This relationship, often called the system transfer function, can be used by an analyst to derive the amplitude and phase of earth motion from the recorded signal or, conversely, to predict the characteristics of a recorded signal that will result from a given input of earth motion. Transfer functions often are listed in tables or graphs that give the steady-state amplitude and phase characteristics of the seismograph with respect to the frequency or period of earth motion. This method of representing the transfer function is adequate for most routine time and amplitude studies. However, a more general mathematical representation of the transfer function or its time domain equivalent, the impulse response, is needed for many computer-based waveform studies. The material that follows in this section deals with the determination of the SRO steady-state response characteristics with emphasis on the procedures used to establish calibration in the absolute sense. The derivation of SRO transfer functions in their more general form is covered in Section 9.0.

The Seismic Research Observatories are calibrated by applying a steady-state, sinusoidal force to the inertial element of each sensor and measuring the amplitude and phase of the resulting signal as recorded on a seismogram or digital tape. This is a widely used method of calibrating seismographs, its chief advantages being simplicity, accuracy, and

generality. The measurements are easy to make and relatively easy to automate, and the data can be reduced rapidly without any special computational aids. Accuracy of the calibration depends on the accuracy in measuring the input and output signals and in determining the forcing constants. Steady-state calibration is equally well suited for the simplest or most complex seismographs, as a knowledge of the active elements in the signal portion of the system is not required.

Normally, calibration signals are applied to a sensor through an electromagnetic transducer mounted between the mass and frame of the instrument. The calibrating force is proportional to the current flowing through the transducer coil. In the case of a pendulum-type instrument the calibrating torque acting on the pendulum is

$$G_c i r_c \sin(\omega t) \quad \text{newton-meters}$$

where G_c is the motor constant of the calibrator, $i\sin(\omega t)$ is the instantaneous current in the calibrator coil, and r_c is the distance along the pendulum from the hinge to the point of application of force. The torque acting on the pendulum due to an acceleration of the earth is

$$Mr_{cm} a \sin(\omega t) \quad \text{newton-meters}$$

where M is the mass of the pendulum, $a\sin(\omega t)$ is the instantaneous acceleration of the frame and r_{cm} is the distance from the hinge to the center of mass. In equating these forcing functions a relationship is established between the peak calibrating current, I, and an equivalent peak earth acceleration, A_{eq}.

$$A_{eq} = \frac{G_c I r_c}{M r_{cm}} \quad \text{meters/second}^2$$

or, in terms of earth displacement,

$$X_{eq} = \frac{G_c I r_c}{M r_{cm} \omega^2} \quad \text{meters}$$

The calibration drive is not restricted to sinusoidal functions. Step functions often are used, although the success in deriving accurate transfer functions from the step response of a seismograph has generally been less than satisfactory.

5.2 SRO Calibration Circuit

Calibration signals are applied to the feedback loop of the SRO sensors. A simplified diagram of the calibration circuit is shown in Figure 5.1. For the sake of clarity some resistive networks, control circuitry, and elements of the feedback loop are not shown. A detailed description of the SRO calibration circuit will be found in the manuals (especially Teledyne-Geotech 1976a, 1976b, and 1976g).

A steady-state calibration signal can be generated from within the SRO system -- the normal procedure -- or derived from an external source. The internal signal generator is a read-only memory (ROM) containing a sine wave stored as 100 equally-spaced digital words. The period of the sine wave is established by the rate at which the digital values are clocked out of the ROM. Twenty-two discrete frequencies can be generated, eleven in the short-period mode, ranging from 0.2 to 20 Hz, and eleven in the long-period mode, ranging from .01 to 1 Hz. The digital words clocked out of the ROM are converted to analog voltages by one of the two digital-to-analog converters (DACs) available in the system. One DAC is located within the downhole seismometer package, the other is contained in the calibrator portion of the Test Set/Controller. During normal operation

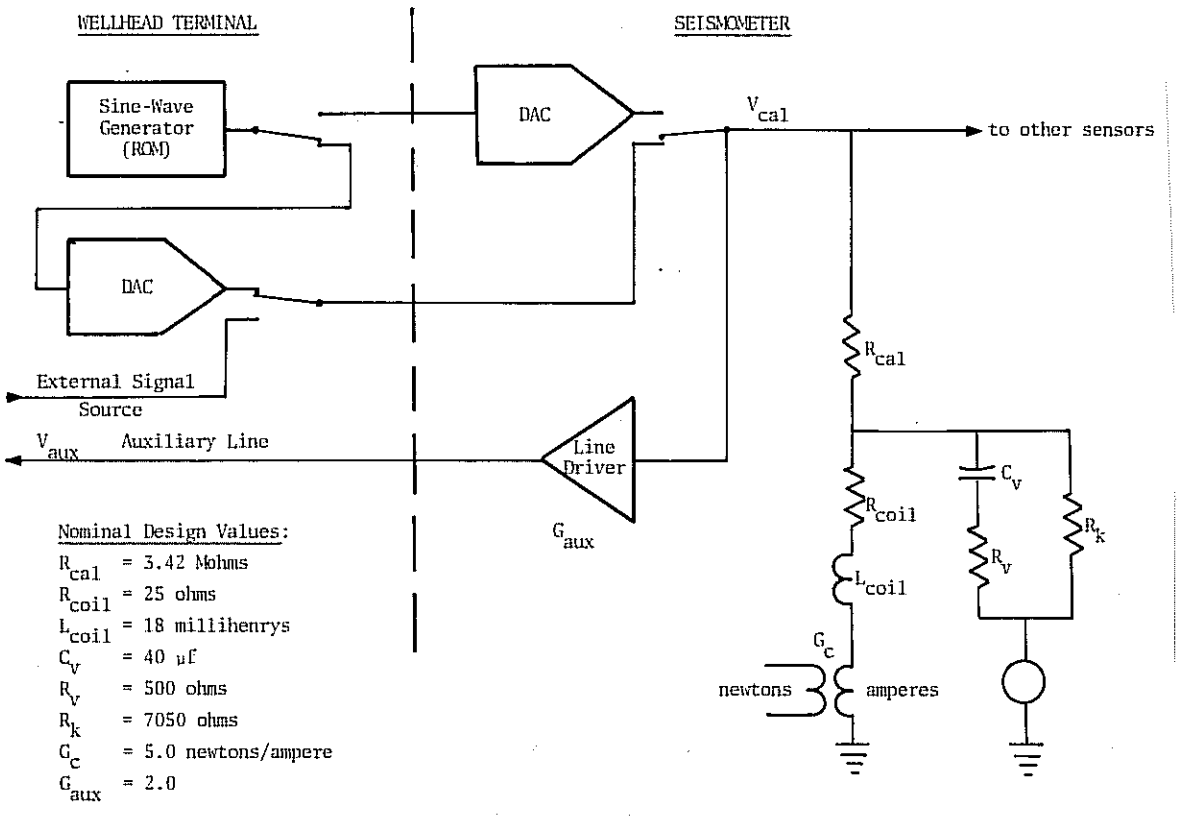

Figure 5.1.--Simplified diagram of the SRO calibration circuit.

the uphole DAC is used to generate the calibration signal, which is then transmitted as an analog voltage to the seismometer. The downhole DAC is used primarily for special tests during installation and maintenance. There are five calibration levels available ranging from 0 to 24 dB in 6 dB steps. The calibration procedures were designed by the manufacturer to facilitate automation and remote control. The calibration drive can be switched on and off by transmitted digital commands.

The calibration voltage is applied simultaneously to all three sensors through precision calibration resistors. The force acting on the mass at the

point of application is proportional to $G_c V_{cal}/R_{cal}$. The precise value of the motor constant is measured at the factory during preassembly tests, then the calibration resistor is selected to produce a basic calibration sensitivity of

$$\frac{A_{eq}}{V_{cal}} = 3.95 \times 10^{-6} \text{ meters/second}^2\text{/volt}$$

or, in terms of equivalent earth displacement,

$$\frac{X_{eq}}{V_{cal}} = \frac{3.95 \times 10^{-6}}{\omega^2} \text{ meters/volt}$$

The calibrating voltage, V_{cal}, is determined by monitoring the voltage, V_{aux}, appearing on the auxiliary circuit during a calibration. The gain of the line driver, G_{aux}, is determined with precision for each seismometer during manufacture and verified as part of the installation and maintenance tests.

For maximum accuracy in computing equivalent earth motion, a frequency-dependent correction must be made to account for the division of calibrating current between the sensor coil and the feedback network (see Figure 5.1). If I* is the effective calibrating current through the coil, for nominal circuit values

$$\frac{I^*(s)}{I_{cal}(s)} = \frac{25938(s + 50)}{(s + 47.705)(s + 27283)} \qquad \text{(where } s = j\omega\text{)}$$

The corrections for amplitude and phase as a function of period are shown in Figure 5.2 and may be applied directly to the values computed for equivalent earth motion. The correction is less than 1% in amplitude and

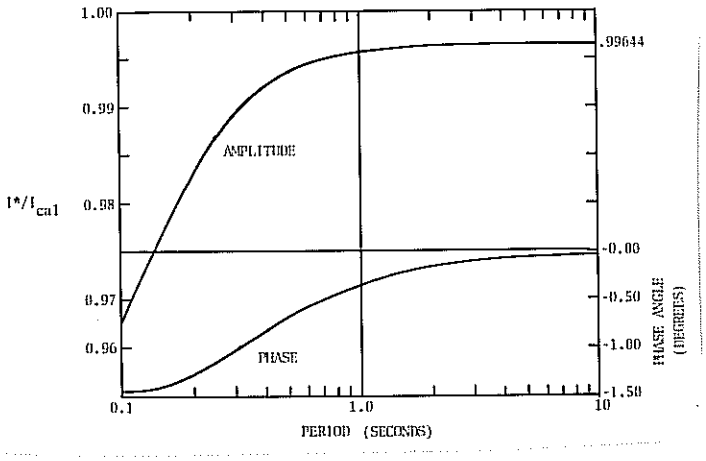

Figure 5.2.--Effective calibration current vs. period. The values should be applied as corrections to V_{cal}/R_{cal}.

and 1 degree in phase for periods greater than .35 seconds.

5.3 SRO Displacement Sensitivity

The absolute sensitivities of the SRO systems with respect to earth displacement are defined at periods of 1 second in the short-period band and 25 seconds in the long-period band. Digital recording sensitivities are adjusted to nominal values of 5,000 digital counts per micrometer in the long-period band and 2,000,000 digital counts per micrometer in the short-period band. At three of the SRO stations (GUMO, SNZO, TATO), the short-period digital sensitivities are set to a nominal value of 2,000 digital counts per micrometer. Normally, the magnification of the long-period seismograms is set at 40,000 at a period of 25 seconds. The magnifications of the short-period seismograms vary from site to site depending upon background levels. Magnifications are listed with the information recorded on the seismograms.

Sensitivities are set at the stations by applying a calibration signal

(at 1 second period in the case of the short-period channel and 25 seconds period in the case of the long-period channels) and adjusting trim attenuators on the seismic filters to produce the required voltage input to the analog-to-digital converter and the required deflection on the seismogram. The long-period calibration signal used during the adjustment is equivalent to an earth displacement of 1.05 micrometers. The short-period calibration signal levels vary from station to station; they are listed in Table 5.1. The displacement sensitivities are adjusted at the stations to within 5% of the nominal values. More precise values for the station sensitivities are determined during data review and are listed in the data files of the network-day tapes.

During day-to-day operation, the SRO systems are automatically calibrated with signals of 1 second and 25 seconds period to permit continuous verification of the absolute displacement sensitivities. A 25-second period calibration signal is applied daily at 0000 hours GMT for 3 minutes. If the long-period data buffer contains any data words larger than 2,048 counts, indicating an event in progress, the daily 25-second calibration is inhibited. During the fifth minute of every fifth day (day numbers 5, 10, 15, etc.), a calibration signal with a period of 1 second is applied unless the event detector is on, indicating a short-period event in progress. On the first short-period calibration day of each month, two additional calibration frequencies in both the long- and short-period bands are run to form a monthly three-point automatic frequency response check. Automated calibration times, periods, and equivalent input amplitudes are listed in Table 5.1

The accuracy of the SRO calibration, in an absolute sense, depends upon factory tests and adjustments, the accuracy in measuring the auxiliary line voltage during a calibration, and the accuracy in measuring the recorded

Station Code	25 second (LP) Calibration Level (micrometers)	1 second (SP) Calibration Level (micrometers)	100 second (LP) Calibration Level (micrometers)	15 second (LP) Calibration Level (micrometers)	5 second (SP) Calibration Level (micrometers)	0.4 second (SP) Calibration Level (micrometers)
ANMO	1.05	.168	8.40	1.512	8.394	0.0538
ANTO	1.05	.672	8.40	1.512	8.394	0.0538
BCAO	1.05	.168	8.40	1.512	8.394	0.0538
BOCO	1.05	.672	8.40	1.512	8.394	0.0538
CHTO	1.05	.168	8.40	1.512	8.394	0.0538
GRFO	1.05	.672	8.40	1.512	8.394	0.0538
GUMO	1.05	1.344	8.40	1.512	16.79	0.215
MAIO	1.05	.336	8.40	1.512	8.394	0.0538
NWAO	1.05	.672	8.40	1.512	8.394	0.0538
SHIO	1.05	.336	8.40	1.512	8.394	0.0538
SNZO	1.05	1.344	8.40	1.512	16.79	0.215
TATO	1.05	1.344	8.40	1.512	16.79	0.215
Time of Occurrence	Daily from 0000 to 0003 GMT	Every fifth day (called an SP calibration day) from 0005 to 0006 GMT	The first SP calibration day of each month from 0105 to 0112 GMT	The first SP calibration day of each month from 0113 to 0117 GMT	The first SP calibration day of each month from 0118 0120 GMT	The first SP calibration day of each month from 0121 to 0122 GMT
Date Implemented	1 January 1977	1 January 1977	Planned for 1 April 1980	Planned for 1 April 1980	Planned for 1 April 1980	Planned for 1 April 1980

Table 5.1.--List of automated calibration levels and times at SRO stations.

calibration signal. It does not depend upon the response characteristics or gain settings of active components in the signal circuits. Any changes in sensitivities or gain settings that might be caused by instability or mishap would be detected during data review.

Once installed, the SRO seismometers are not accessible for hands-on testing, so several important tests and adjustments must be performed at the factory prior to complete assembly of the instrument. First, the motor constant of the electromagnetic transducer must be accurately determined. This is done before the sensor modules are sealed and evacuated. While monitoring the output of the capacitive signal transducer, the pendulum is offset by a known force, then returned to electrical zero by applying a current through the electromagnetic transducer. In the case of the vertical-component sensor, the force is applied by putting a 30 mg weight on the mass. Then the motor constant is computed from the relationship

$$G_c = \frac{mgr_m}{Ir_c} \quad \text{newtons/ampere}$$

where m is the test mass, g is gravitational acceleration, r_m is the distance from the hinge to the test weight, I is the restoring current, and r_c is the distance from the hinge to the centerline of the coil. The mean value of the motor constants for the SRO vertical-component sensors is 5.110 newtons/ampere. In the case of the horizontal-component sensors, the offsetting force is applied by tilting the base of the sensor through a small angle (0.5 milliradians). Then the motor constant is computed from the relationship

$$G_c = \frac{Mgr_{cm}\sin\phi}{Ir_c}$$

where M is the mass of the pendulum, ϕ is the angle of tilt, and r_{cm} is the distance from the hinge to the center of mass. The mean value of the motor constants for the horizontal-component sensors is 4.673 newtons/ampere. The motor constants cannot be measured conveniently after the seismometer is assembled. Early in the program there was an opportunity to verify the stability of the motor constants when a significant percentage of the sensor modules were returned to the factory for internal modifications and the measurements were repeated. Except in those modules where changes were made that affect the transducer sensitivity, the repeatability of the measurements were within 1% (R.D. Wolfe, personal communication).

With the motor constants known, the calibration sensitivities of all the modules are standardized to a common value by adjusting the resistance (R_{cal} in Figure 5.1) in the calibration circuit. The appropriate resistance is computed from the relationship

$$R_{cal} = G_c \times .685 \times 10^6 \text{ ohms}$$

and a calibration resistor is selected to within 1% of this value. This

provides a standard calibration sensitivity of 3.95×10^{-6} meters/second^2/volt.

Other important tests at the factory involve the determination of the level of calibration voltage, V_{cal}, generated by the downhole DAC and the gain of the auxiliary line driver. The results of these tests are provided in the customer data sheet that accompanies the seismometer. The mean value of the calibration voltage at the 0 dB level is 3.556 volts and the maximum deviation has been $\pm$ 0.8%. The mean value of the line driver gain is 1.987 and the maximum deviation has been $\pm$ 0.8%. These values cannot be measured individually after the seismometer is assembled. However, the line driver gain is measured during acceptance, installation, and maintenance testing by assuming that the downhole DAC output is constant, i.e., the two values are measured together. Variations with time (in many cases over a period of years) have been less than $\pm$ 0.6%, which indicates that neither the DAC output nor the line driver gain is varying significantly from the original values provided by the manufacturer. Hence, calibration voltage can be determined to a precision of $\pm$ 1% or better.

In normal operations, including daily calibration, the calibration voltage is derived from the uphole DAC. The stability of this voltage output, based on tests made during acceptance, installation, and maintenance, is $\pm$ 0.9% in the long-period mode and $\pm$ 1.05% in the short-period mode.

During data review at the Albuquerque Seismological Laboratory, selected long-period and short-period calibration signals are displayed on a terminal and scaled. A facsimile of the display showing peak-to-peak values in digital counts is filed with each tape log. The stability of these calibration signal measurements are remarkable as the variations (a preliminary study shows $\pm$ 2% for the long-period signals and $\pm$ 1.5% for the

short-period signals) are considerably less than the temporal variations in background noise levels. This attests to the stability of all of the components in both the calibration and signal circuits of the SRO system.

5.4 Frequency Response Measurements

The sine-wave calibrator in the Test Set/Controller is used to determine the amplitude frequency response characteristics of the SRO components routinely during both installation and scheduled maintenance. Short-period data points are taken at 0.2, 0.5, 1.0, 1.5, 2.0, 2.5, 3.0, 4.0 and 5.0 Hz; long-period data points are taken at periods of 10, 15, 20, 25, 30, 40, 50, 60, 80, and 100 seconds. The analog data are reduced on site and included in the installation and maintenance reports; the digital data are analyzed at the Albuquerque Seismological Laboratory. As one would expect, the precision of these measurements is greatest at the mid-band frequencies where the calibration signal-to-noise ratio is highest but measurement error increases at the band edges. Nominal amplitude response curves are shown in Figures 5.3 through 5.6 for the short-period channel and three configurations of the long-period channels. Each plotted point on the amplitude response curves represents the mean measured value and the solid curves are computed from the transfer functions derived in Section 9.0. Since phase angles are not normally measured during routine installation and maintenance testing, the points on the phase response curves were derived from measurements taken on a test system at Albuquerque. Differences between measured and computed values for both amplitude and phase are shown with the curves.

While the routine tests provide sufficiently accurate calibration data for most purposes, both amplitude and phase measurements over a wider band are needed to derive the transfer functions for individual components. This led to the development of special calibration procedures in which an external

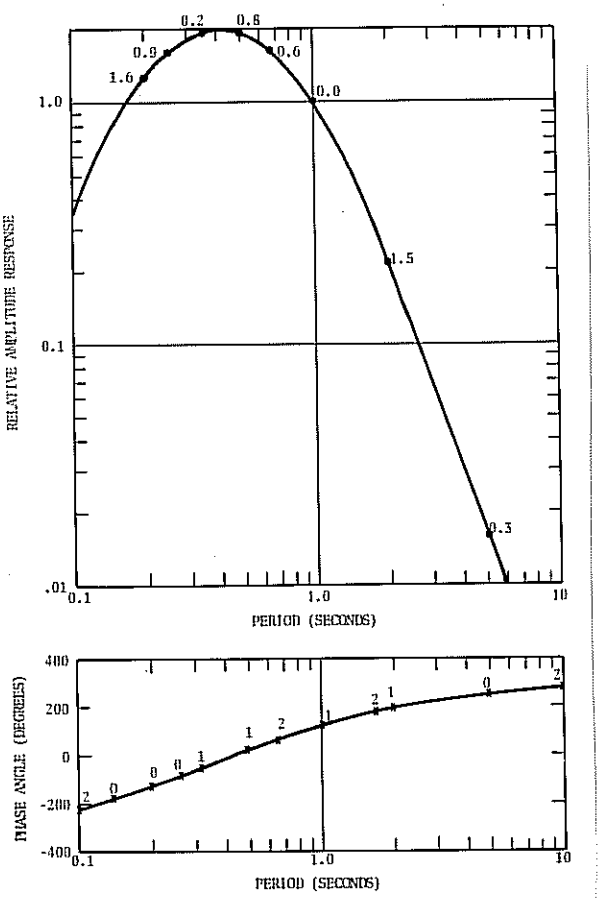

Figure 5.3.--Nominal short-period digital and analog amplitude and phase response to earth displacement. Solid lines are derived from nominal transfer function (see Section 9.0). Measured amplitude points represent mean values of minimum of 21 samples taken from 9 sensors. Phase measurements were taken from test system. Differences between measured and computed points are given in percent of deviation for amplitude and degrees for phase.

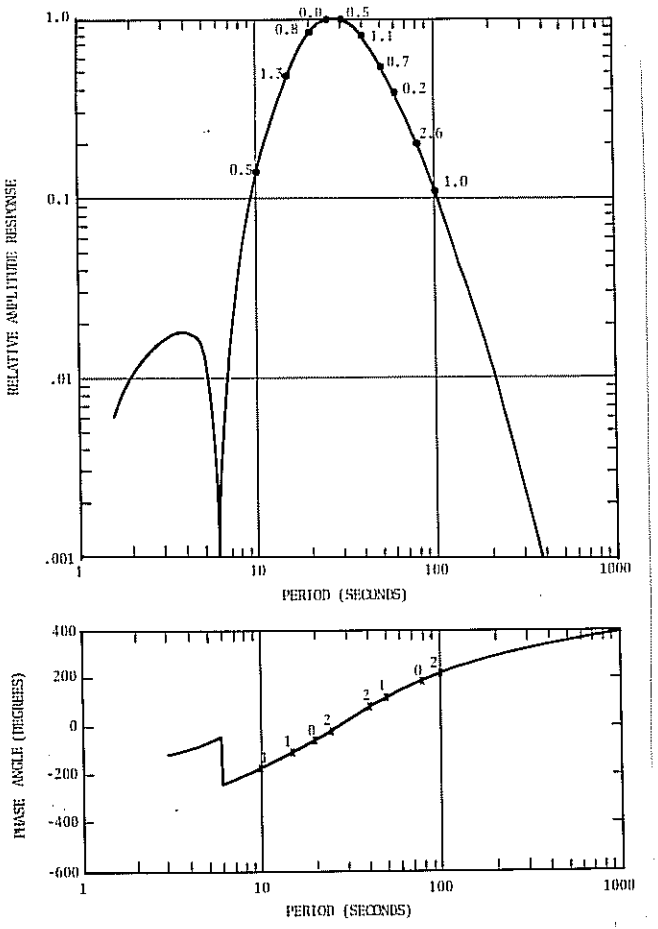

Figure 5.4.--Nominal long-period analog amplitude and phase response to earth displacement. Solid lines are derived from nominal transfer function (see Section 9.0). Measured amplitude points represent mean values of minimum of 21 samples taken from 21 sensors. Phase measurements were taken from test system. Differences between measured and computed points are given in percent of deviation for amplitude and degrees for phase.

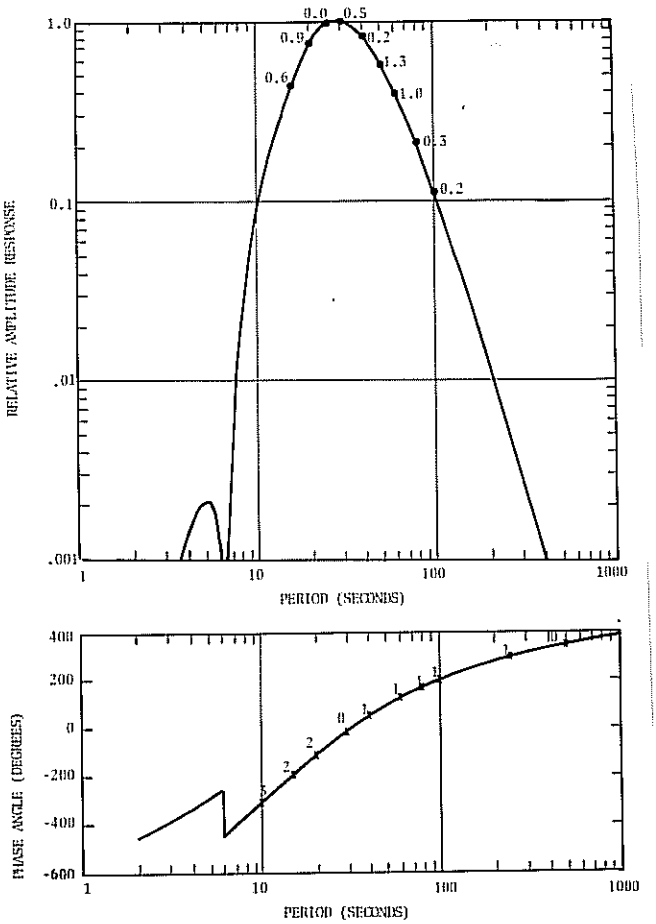

Figure 5.5.--Nominal long-period digital (Bessel) amplitude and phase response to earth displacement. Solid lines are derived from nominal transfer function (see Section 9.0). Measured amplitude points represent mean values of minimum of 14 samples taken from 14 sensors. Phase measurements were taken from test system. Differences between measured and computed points are given in percent of deviation for amplitude and degrees for phase.

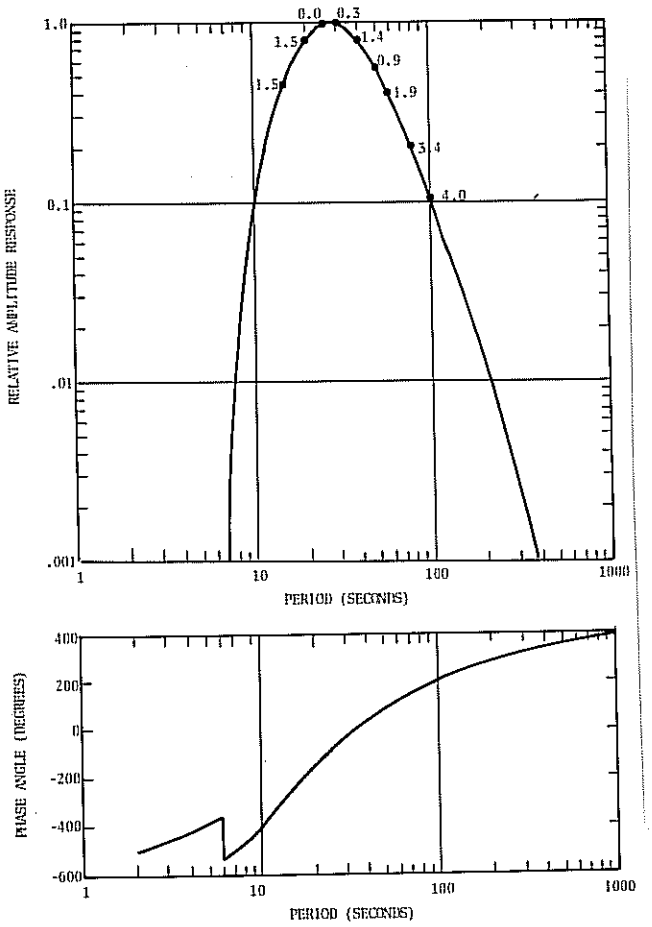

Figure 5.6.--Nominal long-period digital (Butterworth) amplitude and phase response to earth displacement. Solid lines are derived from nominal transfer function (see Section 9.0). Measured amplitude points represent mean values of minimum of 9 samples taken from 9 sensors. Differences between measured and computed points are given in percent of deviations. Good measured phase data are not available.

signal source is used so that the signal-to-noise ratio can be improved at the band edges. The calibration and output signals are recorded on a two-channel digital oscilloscope. The 12-bit digitizer in the oscilloscope permits a measurement precision of .05%. In practice, with noise present in the output signal, precision is estimated to be 0.1% at mid band and 1% at the band edges, based on repeatability of measurements. The phase angle is computed from the time lag between the input and output waveforms. During the test the digitizing rate is set such that 512 samples per cycle are recorded, so the measurement precision of the phase measurements is 0.7^{o}. With noise present, precision is 1.4^{o} at mid band and 2.8^{o} at the band edges, based on repeatability of measurements. The special calibration measurements are taken at the vertical mass position output, the data outputs for all three channels, at the seismic filter outputs, and at the anti-aliasing filter outputs. To date, these tests have been completed on only the Albuquerque SRO system (results are given in Section 9.0). All of the SRO systems will be similarly tested.

6.0 SRO SYSTEM NOISE TESTS

6.1 Sensor System Noise Tests

The need for resolving signals at the level of earth background noise in the long-period band places severe limits on the noise that may be generated within the SRO system. Most of the concern and testing has focused on the long-period band because earth background acceleration levels are much lower in the long-period band (at a quiet site, some 40 dB lower at 30 seconds than at 1 second) and because instrument noise typically increases with increasing period. Early in the SRO program several tests were performed to determine the level of instrument noise in the long-period band. Thereafter, noise was evaluated by operating each SRO seismometer in a comparison test with the standard system. Early testing revealed noise in some systems which was generated by noisy electronic components on the loop boards. The level of noise was too low to be detected at the manufacturer's plant but high enough to be visually detected during acceptance testing at the seismically quieter Albuquerque site. A special device called a module simulator was designed and built by the manufacturer for testing the electronic boards at very low signal levels. Marginal components were screened out during the simulator test and there have been very few instances of noisy seismometers since. Although the level of short-period instrumental noise has not been measured directly, the visual coherence achieved in comparative tests with other SRO systems and other types of short-period instruments supports the conclusion that instrumental noise in the short-period visual band is well below the level of earth noise at the quietest sites. Other principal

conclusions derived from the tests described below are that 1) instrumental noise in the SRO long-period band is well below the levels of ambient earth noise, and 2) there exists an environmental noise of undetermined origin external to the seismometer having an amplitude that can exceed earth noise at periods longer than 50 seconds.

Noise generated in the SRO seismometer cannot be measured directly; that is, by a blocked-mass test often used for evaluating noise in conventional seismographs. The alternate method used for evaluating noise in the SRO seismometer is based on the measurement of coherence between two instruments operated in parallel. In a first test, described by Holcomb (1975), two horizontal sensors were operated in parallel within the same borehole seismometer. This test permits a measurement of incoherent noise generated within the seismometer. In a second test, two seismometers were operated in adjacent boreholes with all three components in parallel. This test permits an evaluation of the level of incoherent noise generated outside the seismometer.

The first test, Test A, was performed using an engineering model of the borehole seismometer that had been reconfigured so that the two horizontal sensors operated in parallel. A typical set of test data in the period range from 10 to 100 seconds acquired during a quiet period is shown in Figure 6.1. Power spectral density curves for the two sensors are shown at the top of the figure (they nearly overlay on another) and the coherence function is shown at the bottom. The very high level of coherence in this band clearly indicates that instrument noise is well below earth noise, assuming that there is no common noise source. To check for a common noise source the coherence was measured between the vertical and a horizontal sensor for the same time period. The coherence, shown in

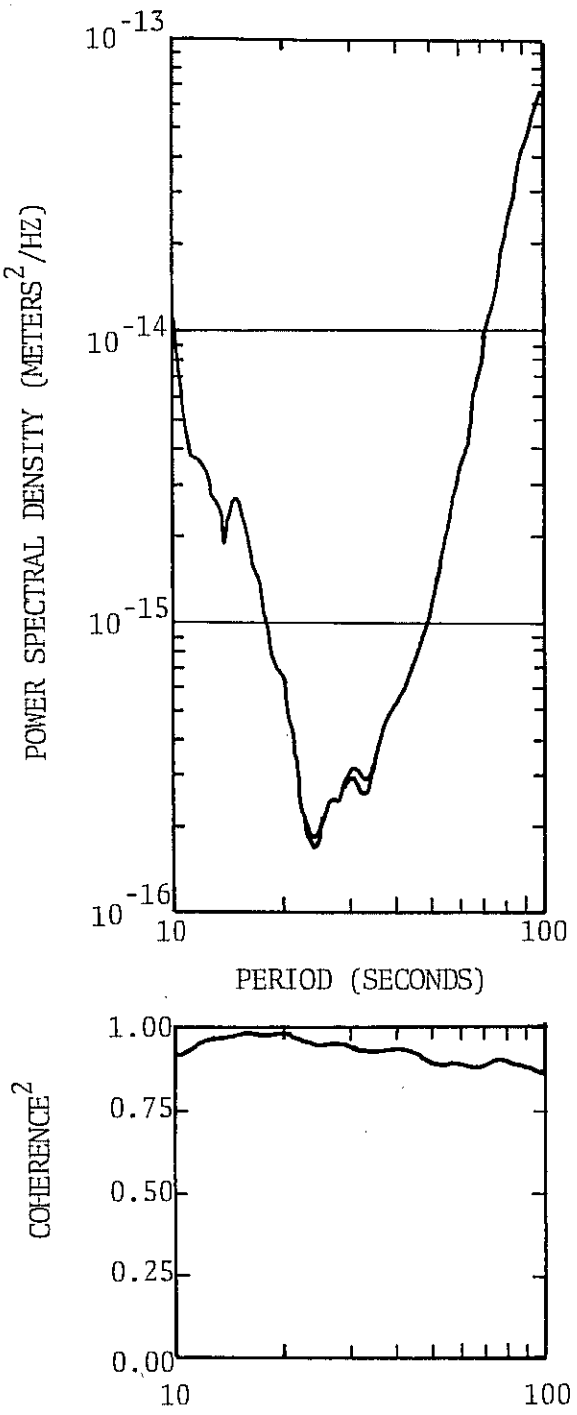

Figure 6.1.--Plots showing power spectral density and coherence functions computed from simultaneous data taken from two horizontal sensors operated in parallel in the same seismometer package.

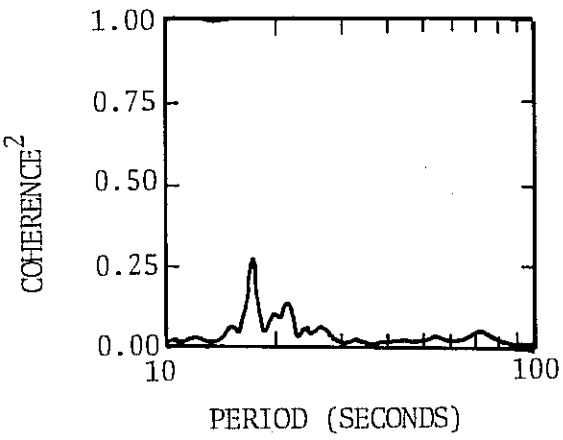

Figure 6.2.--Coherence function computed from simultaneous data taken from two orthogonal sensors operated in the same seismometer package.

Figure 6.2, is nearly zero outside the microseismic band, indicating that a common noise source, such as the power supply, can be discounted.

The level of instrument noise can be determined explicitly from the coherence measurements. A simplified test schematic for Test A (two parallel sensors in the same borehole package) is shown in Figure 6.3. In this

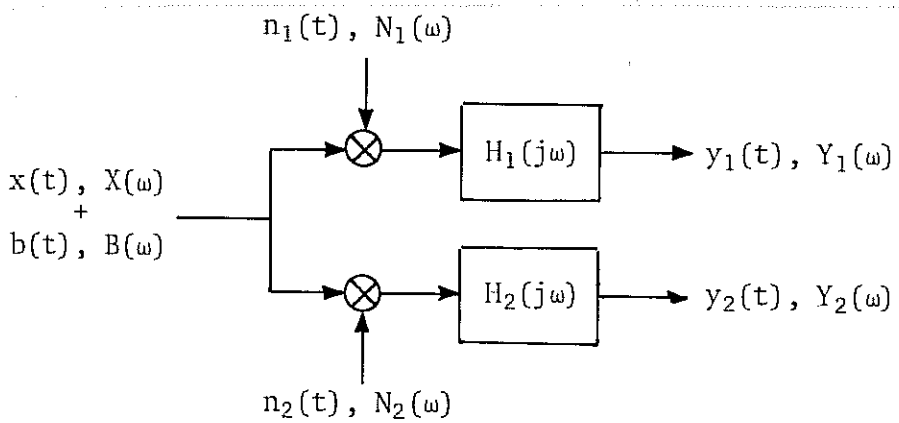

Figure 6.3.--Simplified schematic for Test A.

schematic x(t) and its power spectral density function, $X(\omega)$, represent earth motion; n(t) represents noise originating in the instrument; b(t) represents environmental noise originating outside the instrument; $H_1(j\omega)$

and $H_2(j\omega)$ are the sensor transfer functions; and $y_1(t)$ and $y_2(t)$ are the sensor outputs. System equations can be written:

$$Y_1(\omega) = |H_1(j\omega)|^2\{X(\omega) + B(\omega) + N_1(\omega)\}$$

$$Y_2(\omega) = |H_2(j\omega)|^2\{X(\omega) + B(\omega) + N_2(\omega)\}$$

and, since the signals x(t) and b(t) are coherent at the two outputs, the cross-spectral density function is

$$Y_{12}(j\omega) = H_1(j\omega)H_2^*(j\omega)\{X(\omega) + B(\omega)\}$$

One simplification in the test schematic deserves explanation. The internal noise, n(t), is not necessarily generated at the input. More than likely, the noise is incrementally partitioned by a number of active sections in the system, two of which are shown in Figure 6.4. If in this

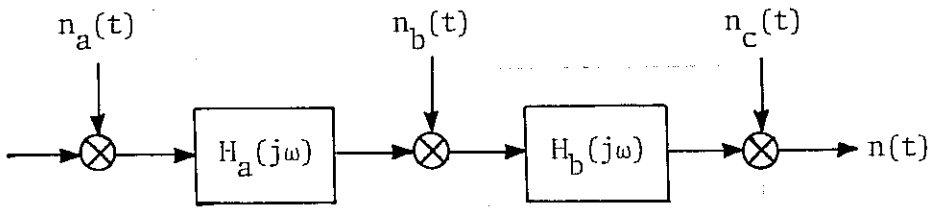

Figure 6.4.--Partitioning of instrument noise.

figure we consider only the noise (no input signal), the output power spectral density function will be

$$N(\omega) = N_c(\omega) + |H_b(j\omega)|^2 N_b(\omega) + |H_a(j\omega)|^2 |H_b(j\omega)|^2 N_a(\omega)$$

If we correct the output for instrument response, then

$$\frac{N(\omega)}{|H_a(j\omega)|^2 |H_b(j\omega)|^2} = N_a(\omega) + \frac{N_b(\omega)}{|H_a(j\omega)|^2} + \frac{N_c(\omega)}{|H_a(j\omega)|^2 |H_b(j\omega)|^2}$$

The right hand side of this equation can be defined as the total instrument noise, $N(\omega)$, referred to the input, and there could be any number of active sections involved. Note that in correcting for instrument response, any noise generated in later stages of the system will increase at the output with respect to input signals at frequencies that lie outside the passband, that is, when the values of the transfer functions are less than 1 in a relative sense.

Based on the similarity of the two power spectral density curves shown in Figure 6.1, it is valid to assume that the noise generators within the separate instruments, while statistically independent, produce equal levels of noise power; that is, $N(\omega) = N_1(\omega) = N_2(\omega)$. The coherence function, γ_{12}^2, is defined as

$$\gamma_{12}^2 = \frac{|Y_{12}(j\omega)|^2}{Y_1(\omega)Y_2(\omega)} = \frac{1}{1 + \frac{2N(\omega)}{X(\omega) + B(\omega)} + \frac{N(\omega)^2}{\{X(\omega) + B(\omega)\}^2}}$$

We can define a signal-to-noise ratio (SNR) as the ratio of coherent to non-coherent signal, that is

$$SNR = \frac{X(\omega) + B(\omega)}{N(\omega)}$$

Then we can compute SNR from the coherence function using the relation

$$SNR = -\frac{1}{\left(1 - \frac{1}{\gamma_{12}^2}\right)} \pm \left[\frac{1}{\left(1 - \frac{1}{\gamma_{12}^2}\right)^2} - \frac{1}{\left(1 - \frac{1}{\gamma_{12}^2}\right)}\right]^{\frac{1}{2}}$$

(ignoring negative values of SNR). The signal-to-noise ratio computed

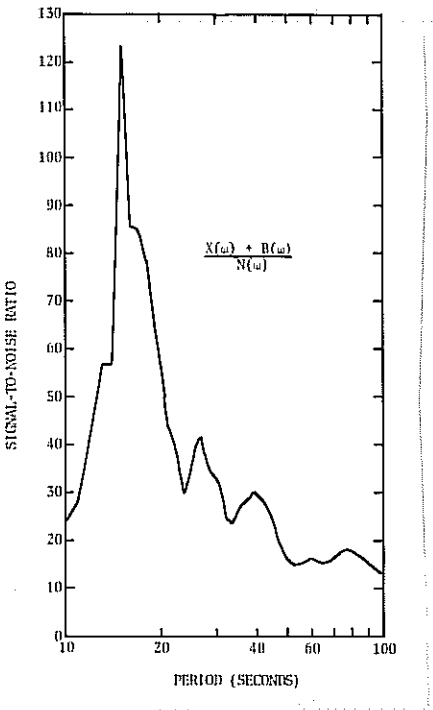

Figure 6.5.--Signal-to-noise ratio computed from coherence function shown in Figure 6.1 (two sensors operated in parallel in same hole).

from the coherence data given in Figure 6.1 is plotted in Figure 6.5. The minimum SNR is 12 dB in the 10 to 100 second period band and 20 dB in the 20 to 40 second period band. It is interesting to note the sharpness of the 27-second microseismic peak although this energy is not especially noticeable in the power spectral density curves. Since

$$\frac{Y(\omega)}{|H(j\omega)|^2} = X(\omega) + B(\omega) + N(\omega)$$

the noise power can be calculated from the relationship

$$N(\omega) = \frac{Y(\omega)}{|H(j\omega)|^2(SNR + 1)}$$

Both the noise power and the coherent signal power are plotted in Figure 6.6.

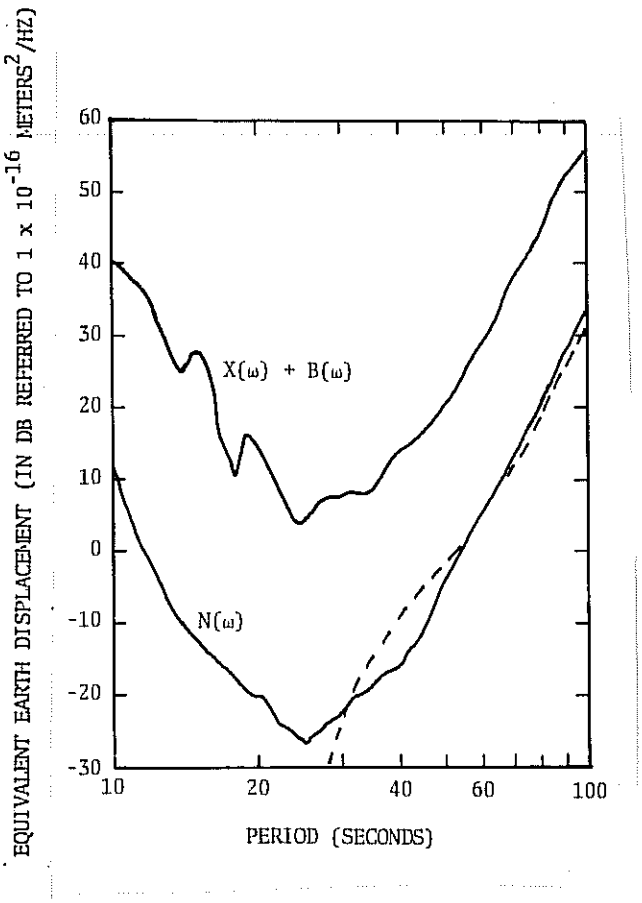

Figure 6.6.--Power spectral densities of coherent and non-coherent signals computed from coherence function shown in Figure 6.1. Dashed line represents noise measured by Sherwin and Kraus (1974).

The dashed line in the figure represents noise measured by Sherwin and Kraus (1974) in a bench test of the KS vertical module. The fact that the noise curve follows the inverse system response at periods shorter than 25 seconds would indicate that noise was being generated in the later stages of the test system, after the response-shaping filters. Clearly, however, the level of instrument noise is well below the coherent signal throughout the 10 to 100 second period band.

In the second test, Test B, two seismometers were operated at the same depth in separate boreholes spaced about 25 meters apart. In fact, this test has been repeated for every seismometer used in the program. The data acquired during a quiet period in the first such test (the only data

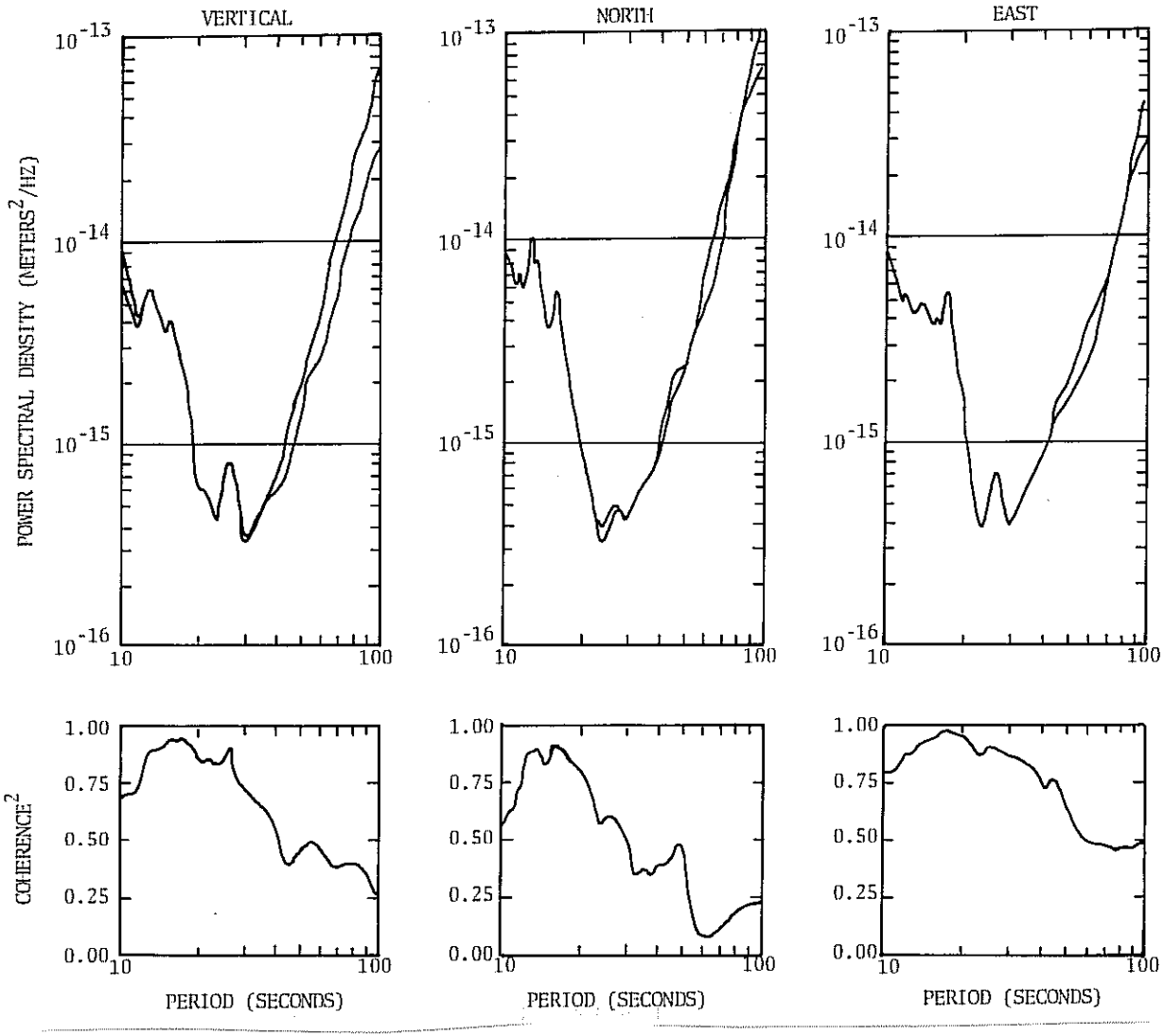

Figure 6.7:--Plots showing power spectral densities and coherence functions computed from simultaneous data taken from vertical and horizontal sensors operated in parallel in adjacent boreholes.

that have been analyzed in detail thus far) are shown in Figure 6.7. The reduced level of coherence between the parallel outputs in this test is assumed to be caused by a noise source external to the seismometer, perhaps associated with the borehole environment. Also, the power spectral density curves do not match as well as they did in the first test. This could be explained by a difference in the level of environmental noise; the boreholes are not identical, one being deeper than the other.

A simplified schematic for Test B is shown in Figure 6.8. In this case,

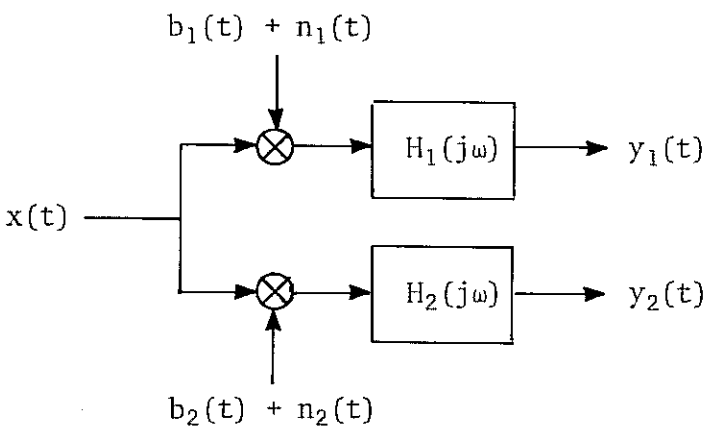

Figure 6.8.--Simplified schematic for Test B.

x(t) is the only common signal and both b(t) and n(t) in the two test systems are statistically independent. The system equations, cross-spectral density, and the coherence function may be written

$$Y_1(\omega) = |H_1(j\omega)|^2 \{X(\omega) + B_1(\omega) + N_1(\omega)\}$$

$$Y_2(\omega) = |H_2(j\omega)|^2 \{X(\omega) + B_2(\omega) + N_2(\omega)\}$$

$$Y_{12}(j\omega) = H_1(j\omega)H_2^*(j\omega)X(\omega)$$

$$\gamma_{12}^2 = \frac{|H_1(j\omega)|^2 |H_2(j\omega)|^2 X^2(\omega)}{Y_1(\omega)Y_2(\omega)}$$

From these relationships the power spectral density of earth displacement can be derived immediately as

$$X(\omega) = \gamma_{12} \left[\frac{Y_1(\omega) Y_2(\omega)}{|H_1(j\omega)|^2 |H_2(j\omega)|^2} \right]^{\frac{1}{2}}$$

and the incoherent signal, $B(\omega) + N(\omega)$, can be derived as the difference between the corrected output and earth displacement.

Values of the coherent spectra, $X(\omega)$, and mean spectral values of the incoherent signals, $B(\omega) + N(\omega)$, are shown for the three components in Figure 6.9. Also plotted, for reference, is the level of instrumental noise derived from Test A using the engineering model of the KS 36000 seismometer. Mean, smoothed values of the incoherent signal spectra are shown rather than individual spectra for the two boreholes because differences between the individual spectra, although possibly significant, are less than the statistical accuracies estimated for the spectral computations. Further analysis of available data is needed to characterize the environmental noise more precisely and perhaps determine its source. Ideally, Tests A and B would be rerun concurrently so that environmental noise and instrumental noise could be separated. Based on the limited analysis to date, it is possible to state that enviromental noise is significant and can affect resolution of earth signals at periods longer than 50 seconds.

6.2 Recording System Noise Tests

The noise generated in the SRO recording system can be measured directly. Signal circuits are removed from the input to the recording

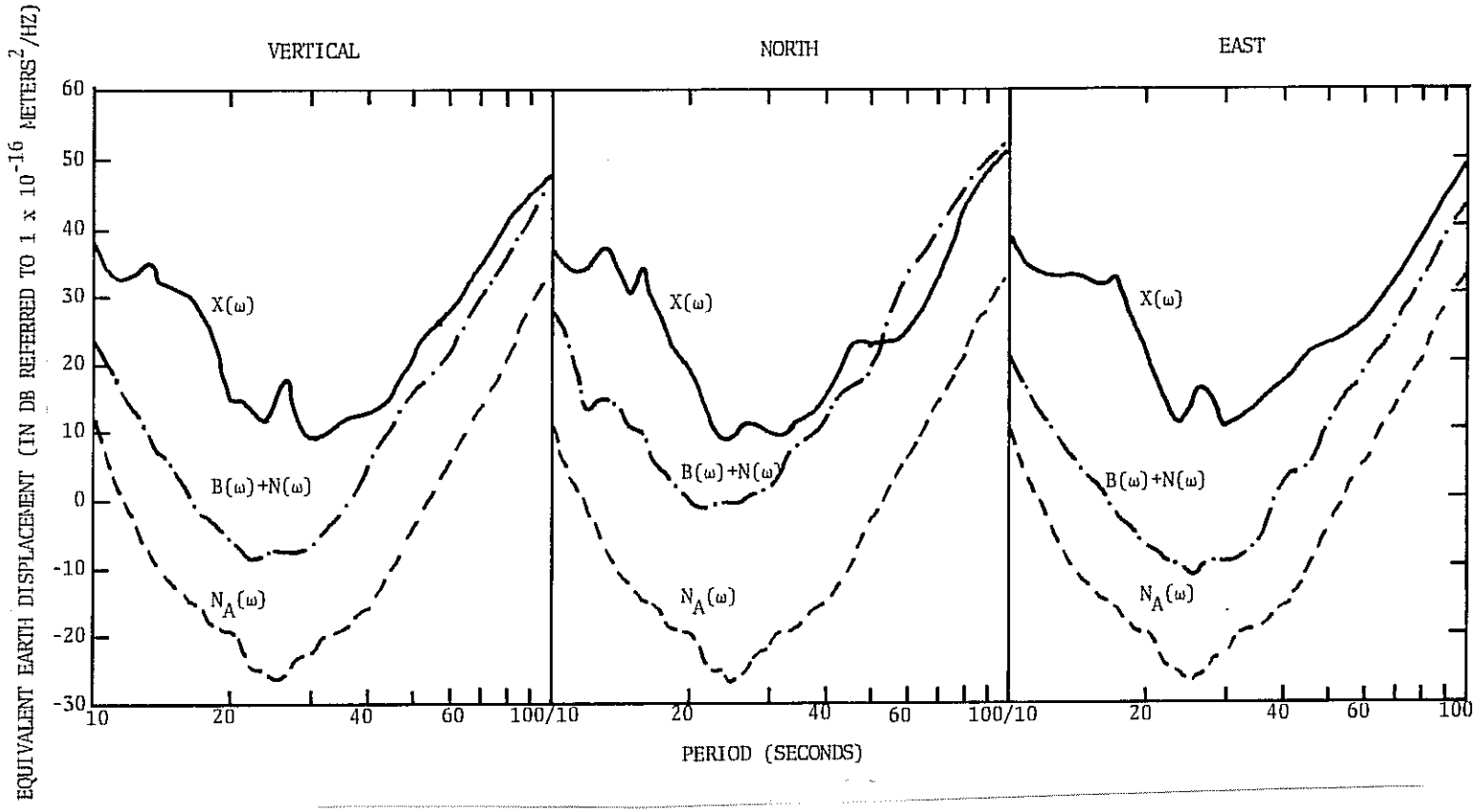

Figure 6.9.--Plots showing power spectral densities of earth noise $X(\omega)$ and incoherent noise $B(\omega) + N(\omega)$ computed from power spectral densities and coherence functions shown in Figure 6.7. Also plotted is the instrumental noise curve $N_A(\omega)$ derived from Test A.

system and replaced by resistors, then the recording system is operated for a period of at least two hours. Two tests are run. The first test includes the seismic filters and all following components. The seismic filters are removed for the second test. This procedures permits an evaluation of the noise in the seismic filters and the recording system.

Typically, the noise level is between 2 and 5 digital counts peak to peak when the seismic filters are not included in the test and between 5 and 10 digital counts peak to peak when they are included. Noise levels above this will prompt corrective action. The recording system noise tests are performed during installation and each scheduled maintenance visit.

7.0 NON-LINEAR DISTORTION

7.1 Clipping Thresholds

Any physically realizable data system has a limited dynamic range and becomes nonlinear when the amplitude of the input signal exceeds the design limit. The amplitude range of possible seismic signals is more than 10 orders of magnitude, say from earth background noise at a quiet site to the amplitudes expected near the epicenter of a large earthquake. No existing single seismometer is capable of producing undistorted output signals over this entire range, so data systems must be designed to meet limited recording objectives.

In the case of the SRO system, the most important objective was the detection of small-amplitude surface waves in the 20 to 40 second period band. Indeed, the justification for using the borehole seismometer was to reduce long-period surface noise. The SRO system was optimized for recording in the 20 to 40 second period band, and, since the level of earth background noise is frequency dependent and the clipping threshold of the instruments relatively constant, the SRO recording range varies with frequency and is less than optimum in other portions of the spectrum. This is illustrated in Figure 7.1. The amplitude range from earth noise to clipping varies from a maximum of about 100 dB at a period of 30 seconds to about 60 dB at a period of 1 second. The recording range in the short-period band at noisy stations would be substantially less but the clipping level at these stations has been raised about 35 dB by using the less sensitive mass position output rather than the data output to drive the short-period filters. SRO clipping thresholds are relatively low in terms of

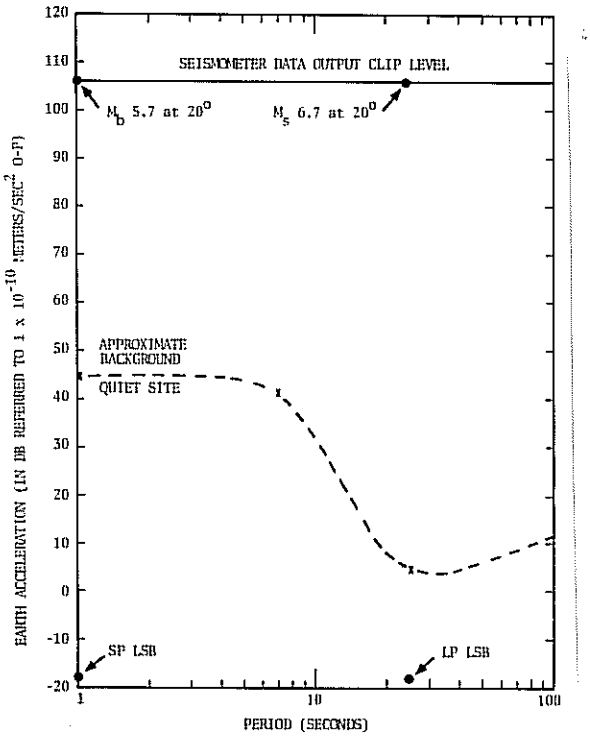

Figure 7.1.--Illustration showing approximate separation of SRO data output clipping level and earth noise at a quiet site.

the earthquake magnitude scale but they could not be raised significantly without losing the ability to resolve earth noise in the long-period band.

SRO clipping thresholds are shown as a function of earth period in Figures 7.2 through 7.4. Clipping levels are given both for the maximum input in units of earth displacement and equivalent output in units of digital counts. Figures 7.2 and 7.3 show the clipping thresholds for the standard long- and short-period channels, and Figure 7.4 shows the clipping thresholds for the stations with modified low-gain short-period channels. At periods above 1 second, the seismometer (more precisely, the data output line drivers) clip when the input of earth acceleration exceeds 4×10^{-5} meters/second^2 peak to peak. In some portions of the band satura-

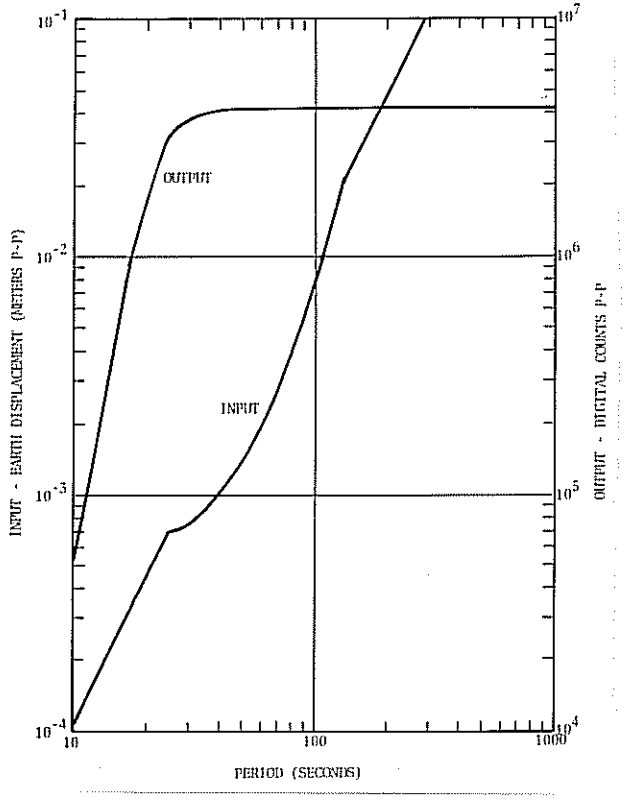

Figure 7.2.--SRO clipping threshold for the long-period channel in terms of both input (earth displacement) and output (digital counts).

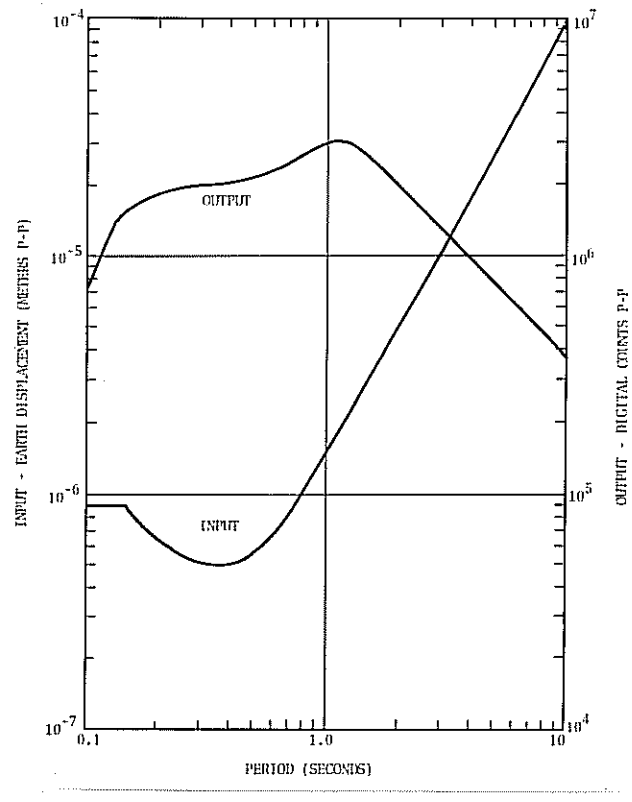

Figure 7.3.--SRO clipping threshold for the standard short-period channel in terms of both input (earth displacement) and output (digital counts).

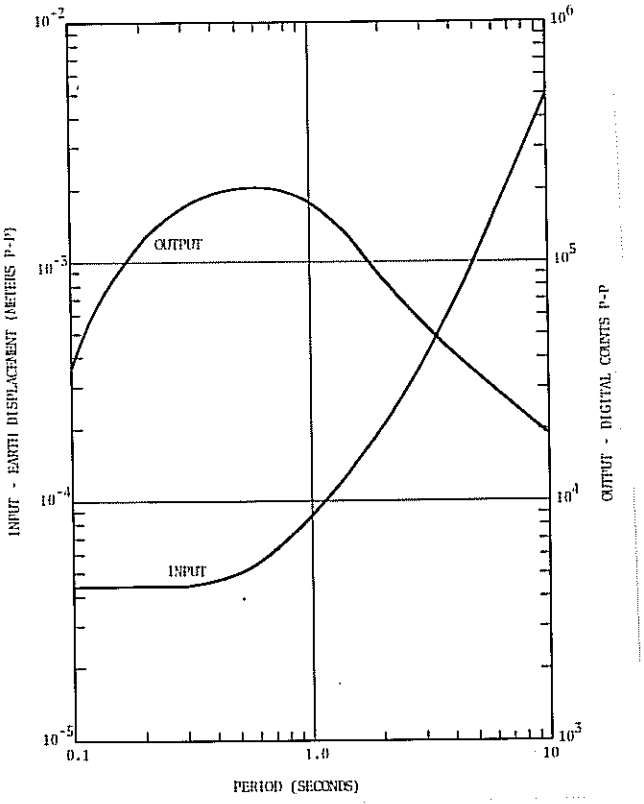

Figure 7.4.--SRO clipping threshold for the special low-gain short-period channel in terms of both input (earth displacement) and output (digital counts).

tion occurs first in the uphole seismic filters or in the analog-to-digital converter. The maximum amplitude of the digital signal is +2,096,128 to -2,097,152 digital counts.

Ideally, clipped signals would have truncated peaks that clearly indicate that clipping has occurred. Unfortunately, this is not always the case for the SRO because of signal conditioning that occurs in the uphole filters. Saturation in the short-period channels causes distortion at the zero crossings rather than a truncation of the peaks because of phase shift in the seismic filters. Often, there is no obvious visual indication that a long-period waveform is distorted because of smoothing that occurs in the low-pass sections of the seismic and anti-aliasing

filters. Analysts should treat very large amplitude long-period signals with caution and compare the signal amplitude with the clip level curve. The clipping levels shown in Figures 7.2 through 7.4 are conservative in order to allow for serious amplitude distortion that can occur as clipping levels are approached. Hard clipping thresholds are measured at periods of 1 and 25 seconds during installation of the station. These levels are at least 20% higher than the values given by the curves. Clipping ambiguities will be eliminated when clip sensors are installed in the SRO systems. These sensors will monitor the data output channel and set flags in the digital records when voltages exceed specified limits.

7.2 Intermodulation Distortion

Clipping, and the amplitude distortion that generally occurs as the system "goes soft" just prior to clipping, can be considered a catastrophic form of non-linear distortion. The effects of non-linear system response between clipping thresholds are less obvious, and perhaps more important for that reason. This type of nonlinearity causes spurious signals to appear at the output.

Ideally, the output of an instrument, $y(t)$, has an amplitude relationship with the input, $x(t)$, such that

$$y(t) = a_0 + a_1 x(t)$$

Typically, however, the output contains higher-order terms and the input-output relationship is described by a polynomial with (assumed) constant coefficients, such that

$$y(t) = a_0 + a_1 x(t) + a_2 x(t)^2 + a_3 x(t)^3 + \ldots\ldots\ldots$$

If the input to a system with this response is the sum of several sinusoidal

terms, say

$$x(t) = A_1 \sin\omega_1 t + A_2 \sin\omega_2 t$$

then the output, considering only the fundamental and quadratic terms, will be

$$\begin{aligned} y(t) = {} & a_1(A_1 \sin\omega_1 t + A_2 \sin\omega_2 t) \\ & + a_2(A_1^2 + A_2^2)/2 \\ & - a_2(A_1 A_2 \cos 2\omega_1 t)/2 \\ & - a_2(A_1 A_2 \cos 2\omega_2 t)/2 \\ & - a_2 A_1 A_2 \cos(\omega_1 + \omega_2)t \\ & + a_2 A_1 A_2 \cos(\omega_1 - \omega_2)t \end{aligned}$$

In addition to the fundamental terms, the output of a system with second-order nonlinearity contains intermodulation distortion products; that is, a DC component, second harmonics of the input frequencies, and sum and difference signals. These distortion products will appear at the output of the system as undesirable noise if the coefficients of the quadratic term has a significant value with respect to the coefficient of the fundamental term. Higher-order terms, if significant, will enrich the intermodulation noise spectrum. In the case of the SRO system, we will assume that cubic and higher-order terms are less significant than the quadratic term,

The level of second-order non-linear distortion in the SRO seismometer is measured using a "two-frequency test" devised by Teledyne Geotech Corporation to measure distortion in seismometers and electronic components. In this test two sine waves of equal amplitude and with nominal frequencies of 1.00 and 1.02 Hz are summed and applied to the seismometer calibration circuit. The maximum peak-to-peak value of the fundamental signal output,

$y_f(t)$, and the peak-to-peak value of the difference signal output, $y_{\Delta f}(t)$, are measured and converted to equivalent amplitude units. Then the distortion level in decibels is computed from the relationship

$$\text{Distortion Level} = 20 \log \frac{a_2}{a_1} = 20 \log \frac{2y_{\Delta f}(t)}{Ay_f(t)}$$

Typically, in the test A = .45; that is, the input signal drives the system through 45% of its operating range.

At the operating SRO stations the range of measured seismometer distortion levels varies from -64 dB to -84 dB with a mean value of -73 dB. Even in the worst case the level of distortion is such that distortion products could not be resolved in any recording band that contained the fundamental output signal because they are at or below the resolving power of the system. Indeed, a specific study of SRO linearity using broadband data failed to reveal any evidence of non-linear distortion (ENSCO Corp., 1975). As it is, the SRO data are recorded in two separate bands making it possible for the fundamental and difference signals to appear in separate bands. Based on the measured distortion levels we could expect to see noise in the long-period channels generated by large amplitude, spectrally rich body waves. The level of this noise could be significant, perhaps as much as 1,000 to 2,000 digital counts, if the input signal drove the system to full scale. The fact that this noise has not been identified is probably due to the presence of much larger amplitude long-period energy in the body wave.

The two-frequency distortion test is also performed on the long-period filters. The average distortion level measured during these tests is -94 dB and the highest measured distortion level has been -76 dB. The distortion test is not routinely performed on the short-period filters because special

test equipment would be needed at the stations. However, the manufacturer's linearity specifications are the same for both long- and short-period filters. It is highly unlikely that the seismic filters would contribute any resolvable distortion products unless a component becomes defective. Precise linearity measurements are not made routinely at the stations on the analog-to-digital converters, again because special test equipment is required. However, tests at the Albuquerque Seismological Laboratory have shown that the ADC output linearly tracks an input voltage throughout its range to within the accuracy of a least-significant bit (.05%).

8.0 SEISMOMETER ORIENTATION AND POLARITY

The SRO seismometers are physically inaccessible during and after installation, so special procedures were developed for establishing orientation and polarity. Azimuthal orientation is fixed by a sequence of installation procedures. First, the seismometer holelock is lowered to its proper depth and locked to the casing wall using a special installation tool. The holelock is slotted on one side and both the seismometer and installation tools have keys which guide the instruments into the orienting slot in the holelock. After the holelock has been emplaced, a gyroscopic tool is lowered and mated with the holelock to determine the azimuth of the slot. The gyroscopic tool itself is first aligned at the surface on a geographic north reference marker that has been surveyed prior to installation. Three separate runs downhole are made with the orientation tool and the results are averaged. The key at the base of the seismometer is mounted on an azimuth ring that can be adjusted to produce north-south and east-west axes of the horizontal sensors when the seismometer is seated in the holelock. The accuracy of the orientation tool, according to manufacturer specfications, is $\pm$ 1 degree. An orientation accuracy at the stations of $\pm$ 3 degrees appears to be a reasonable assumption based on experience and repeatability of measurements. The orientation tool is shipped to the site for the installation. When it is returned to the Albuquerque Seismological Laboratory, proper operation is verified in a test holelock of known orientation.

The polarity of the signals in the SRO system conform to the conventional practice of having upward excursions on the seismograms and

positive-going values of the digital words signify up, north, and east directions of earth displacement. Signal and calibration polarities within the seismometer, the wellhead terminal, and the interconnecting cables and connectors are fixed during manufacture. During acceptance testing at Albuquerque, factory polarities are checked by comparing data recorded on the test and standard systems. During installation at a station the polarity of the digital recording system is checked by applying a DC voltage to the input of the analog-to-digital converter. All interconnecting cable connections between the seismometer, wellhead terminal, and recording system are documented on an installation form. With proper polarity the initial offset of a sine-wave calibration signal will break down on the seismograms and in a negative direction on tape. At most SRO stations polarity settings can be verified by comparison with conventional seismographs operated nearby.

In spite of precautions there have been two confirmed instances (at BCAO and SHIO) where orientation procedures were not followed correctly during initial installation of the seismometer and the horizontal components have been 180^{o} out of phase. Orientation at SHIO was corrected in September 1978 and orientation at BCAO will be corrected during the next maintenance visit.

9.0 SRO SYSTEM TRANSFER FUNCTIONS

9.1 General

The derivation of transfer functions for the SRO system has progressed more or less in a step-wise fashion with each succeeding step providing more detail and greater accuracy. In fact, this work is still in progress as the goal now is to provide individual transfer functions for each component in the SRO network. McCowan and Lacoss (1978) published the first comprehensive analysis of the SRO system and its transfer characteristics. Their transfer functions essentially describe the manufacturer's intended response characteristics. However, they are not exact solutions for the operating systems because the information available to the authors was incomplete and because the actual working parameters of the system are somewhat different than the design parameters given in the manuals. More recently, Farrell and Berger (1979) derived SRO transfer functions, again based on parametric modeling, but with additional active elements considered. In a companion paper, Berger and others (1979) describe a calibration technique and its application for determining more exact values for several important SRO parameters. The Farrell and Berger transfer functions are more accurate than the McCowan and Lacoss transfer functions but they are incomplete and, to a large extent, still based on design data rather than measured parameters. Our intention in this report is to provide a complete model of the SRO operating system and a set of transfer functions that are verified by steady-state measurements.

There have been several factors complicating the derivation of accurate SRO transfer functions. One has been the large number of active elements in

the system. Some have response characteristics that are predictable from design data; others do not, and their transfer characteristics must be derived by adjusting the polynomials to fit measured data. Another complicating factor is the number of SRO operating configurations. These must be treated separately if accuracies are to be held to 2% or better. The SRO operating configurations are illustrated in Figure 9.1, and the terminology that will be used to describe the different transfer functions is summarized in this figure as well. Recall that the current and past operating configurations at the SRO stations are given in Table 2.1.

It would be well at this point to define several other terms that will be used. What we will call the "design" response is based on design data rather than measured data. A "nominal" transfer function is one that most closely matches the mean value of measured data taken from all SRO systems. A "component" transfer function is one that has been derived for a specific component of an SRO operating system. The component transfer functions are the most accurate and typically agree with the measured data to within 1% to 2% in amplitude and 1^{o} to 2^{o} in phase throughout the band. If component transfer functions are not available, the nominal transfer function for that operating component should be used. The agreement between nominal transfer functions and measured data is illustrated in Figures 5.3 through 5.6. The currently known transfer functions for individual SRO components will be listed in the data logs on the network-day tapes. If the component transfer function is not available, the appropriate nominal transfer function will be listed.

9.2 Seismometer

Although compact and miniaturized, the sensors used in the SRO borehole seismometer were constructed using conventional design: a LaCoste

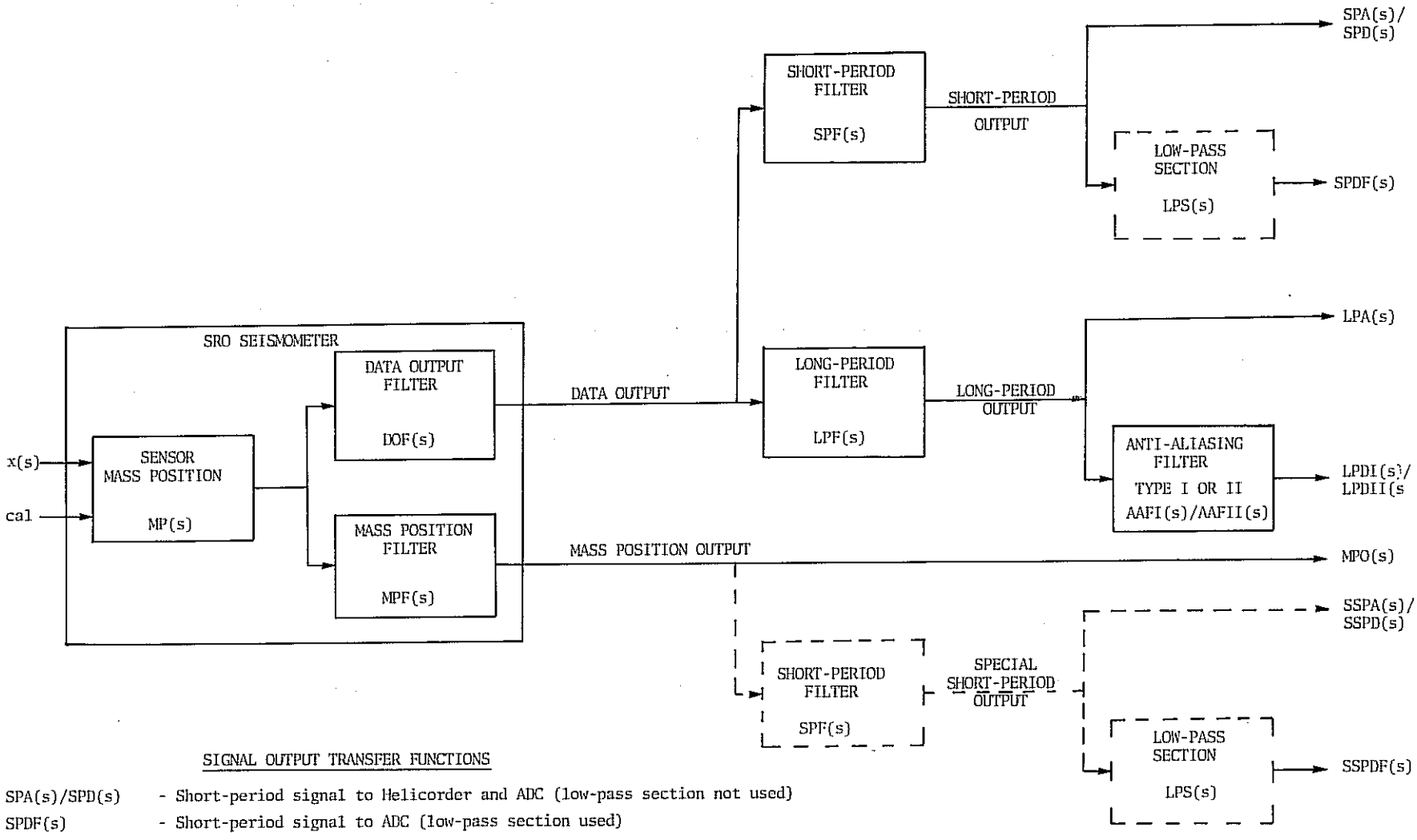

SIGNAL OUTPUT TRANSFER FUNCTIONS

SPA(s)/SPD(s)	- Short-period signal to Helicorder and ADC (low-pass section not used)
SPDF(s)	- Short-period signal to ADC (low-pass section used)
LPA(s)	- Long-period signal to Helicorder
LPDI(s)	- Long-period signal through Type I (Butterworth) anti-aliasing filter to ADC
LPDII(s)	- Long-period signal through Type II (Bessel) anti-aliasing filter to ADC
MPO(s)	- Mass position signal (not currently recorded)
SSPA(s)/SSPD(s)	- Special low-sensitivity short-period signal to Helicorder and ADC (low-pass section not used)
SSPDF(s)	- Special low-sensitivity short-period signal to ADC (low-pass section used)

NOTE: Low-pass sections are being removed at all stations; Butterworth filters are being replaced by Bessel filters at all stations.

Figure 9.1.--Summary of active SRO elements. Only one long-period channel is shown.

suspension is used for the vertical component and "garden-gate" suspensions are used for the horizontal components. Electrical signals are generated by a capacitive transducer mounted between the frame and moving mass. The period and damping of the sensors are controlled by feedback. In open-loop operation the period is between 5 and 10 seconds and the damping is less than 2% of critical; in closed-loop operation the period is close to 1 second and the damping is near critical. The feedback signals and the calibration drive are applied to the moving mass through a coil-magnet transducer.

A block diagram of the active elements in the downhole seismometer package is shown in Figure 9.2. The pendulum, the transducer, and the first-stage amplifier are contained inside the sealed and evacuated sensor module. The demodulators, modulator, and feedback circuit are located on a "loop" board in the electronics section of the downhole package. Signal levels are boosted and the signals are converted from single-ended to differential drive by line drivers, which are also located in the electronics section of the seismometer. The values given in Figure 9.2 are the design values. Electronic component tolerances are held to within 1%. However, mechanical and electromechanical components cannot be held within such close tolerances during manufacture. Both the sensitivity of the capacitive transducer and the motor constant of the coil-magnet transducer vary from design values. For example, the average value of G_c for the vertical sensors is 5.11 newtons/ampere and for the horizontal sensors it is 4.67 newtons/ampere. The resistances selected for R_k and R_{cal} depend upon the value of G_c.

In analyzing the seismometer, using essentially the methods of McCowan and Lacoss (1978), it helps to simplify the circuit using the block diagram shown in Figure 9.3 where a(s) represents earth acceleration and the T(s)'s

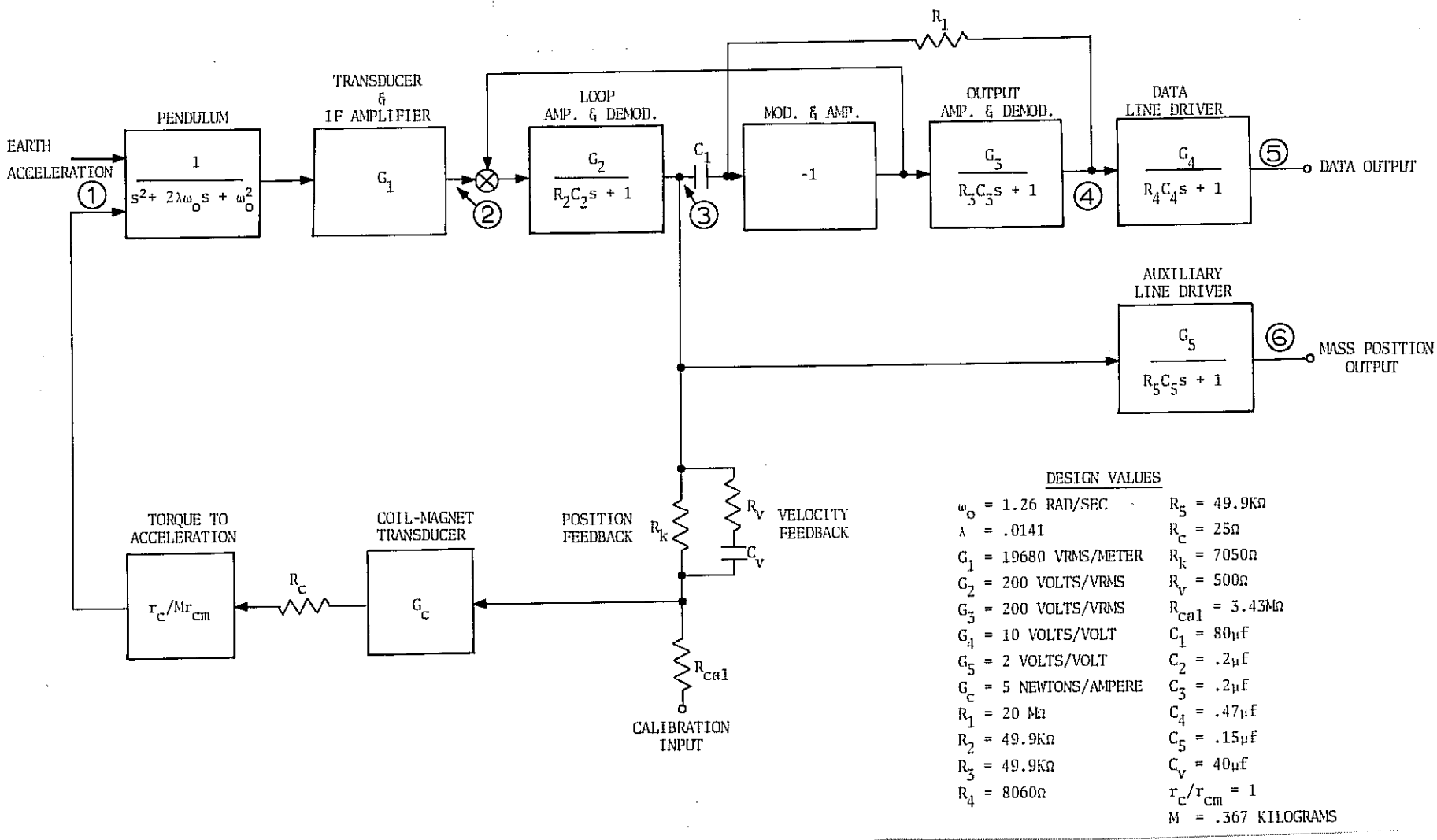

Figure 9.2.-- Block diagram of active elements in downhole seismometer package. The encircled numbers correspond to similar circuit locations in Figure 9.3.

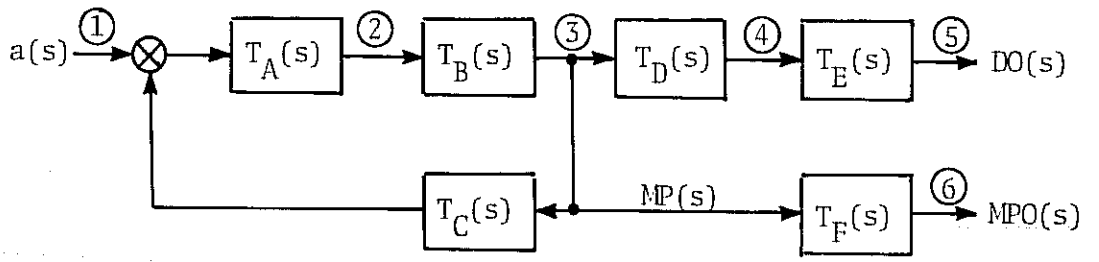

Figure 9.3.--Simplified schematic of downhole circuits.

represent subcomponent transfer functions. The numbered locations in the diagram correspond to the numbered locations in the more detailed circuit of Figure 9.2.

The transfer function $T_A(s)$ represents the sensor and amplified output of the transducer and can be expressed as

$$T_A(s) = \frac{G_1}{s^2 + 2\lambda\omega_o s + \omega_o^2}$$

where ω_o is the open-loop (natural) angular frequency of the sensor and λ is the damping ratio. The element designated $T_B(s)$ provides a first-order attenuation rate of the loop signal between 10,000 and 50 seconds period.

$$T_B(s) = \frac{G_2\{(\tau_1 s + 1)(\tau_2 s + 1) + G_2\}}{(\tau_2 s + G_2 + 1)(\tau_1 s + 1)(\tau_2 s + 1)}$$

where $\tau_1 = R_1C_1$ and $\tau_2 = R_2C_2$. Since $\tau_1 = 1600$ and $\tau_2 = .01$, this can be simplified without significant loss of accuracy to

$$T_B(s) = \frac{G_2(\tau_1 s + G_2 + 1)}{(G_2 + 1)(\tau_1 s + 1)}$$

The transfer function, $T_C(s)$, represents the feedback circuit and the forcing constant of the coil-magnet transducer converted to equivalent

units of acceleration of the frame.

$$T_C(s) = \frac{G_c((\tau_v + \tau_k)s + 1)}{MR_k\{R_c/R_k((\tau_v + \tau_k)s + 1) + \tau_v + 1\}}$$

where $\tau_v = R_vC_v$ and $\tau_k = R_kC_v$. The transfer function to this point can be derived from the component transfer functions using the relation

$$\frac{MP(s)}{a(s)} = \frac{T_A(s)\ T_B(s)}{1 + T_A(s)T_B(s)T_C(s)}$$

so, in general form with the stated approximation, MP(s)/a(s) =

$$\frac{G_1G_2(\tau_1s+G_2+1)\{R_c/R_k((\tau_v+\tau_k)s+1)+\tau_vs+1\}}{(s^2+2\lambda\omega_0s+\omega_0^2)(G_2+1)(\tau_1s+1)\{R_c/R_k((\tau_v+\tau_k)s+1)+\tau_vs+1\}+\frac{G_1G_2G_c}{MR_k}(\tau_1s+G_2+1)((\tau_v+\tau_k)s+1)} \quad V/M/S^2$$

MP(s) is the feedback signal; it cannot be measured at the output of the seismometer.

The two measureable outputs are the data output, DO(s), and the mass position output, MPO(s). The transfer function $T_D(s)$ in the data output channel represents a bandpass filter with design corner frequencies at .02 and 16 Hz and a gain of 200.

$$T_D(s) = \frac{G_3\tau_1s}{(\tau_1s + 1)(\tau_3s + 1) + G_3}$$

where $\tau_3 = R_3C_3$. The final element of the data output channel is the line driver. It is a single-pole low-pass filter with a design corner at 42 Hz and a gain of 10 and can be represented as

$$T_E(s) = \frac{G_4}{(\tau_4s + 1)}$$

where $\tau_4 = R_4C_4$. Then the transfer function for the data output channel is

$$\frac{DO(s)}{a(s)} = \frac{MP(s)}{a(s)} \times T_D(s)T_E(s)$$

or

$$\frac{DO(s)}{a(s)} = \frac{MP(s)}{a(s)} \times \frac{G_3G_4\tau_1 s}{(\tau_4 s + 1)\{(\tau_1 s + 1)(\tau_3 s + 1) + G_3\}} \quad \text{VOLTS/M/S}^2$$

The transfer function $T_F(s)$ in the mass position output channel represents the line driver which is a low-pass filter with a design corner at 21 Hz and a gain of 2.

$$T_F(s) = \frac{G_5}{(\tau_5 s + 1)}$$

where $\tau_5 = R_5C_5$. So the transfer function for the mass position output is

$$\frac{MPO(s)}{a(s)} = \frac{MP(s)}{a(s)} \times \frac{G_5}{\tau_5 s + 1} \quad \text{VOLTS/M/S}^2$$

In terms of design values, the mass position output of the SRO seismometer is

$$MPO(s) = \frac{5.23 \times 10^6 (s + .126)(s + 47.6)a(s)}{(s^2 + 14.7s + 57.1)(s + .120)(s + 32.9)(s + 134)} \quad \text{V/M/S}^2$$

The quadratic expression in the denominator represents the closed-loop design characteristics of the pendulum with a natural frequency of 1.2 Hz and a damping near critical. The zero-frequency mass position sensitivity, for design values, is 1040 volts/meter/second^2. Likewise, for design values, the data output is

$$DO(s) = \frac{1.03 \times 10^{12}(s + 47.6)sa(s)}{(s^2 + 14.7s + 57.1)(s + .120)(s + 32.9)(s + 100)(s + 264)} \quad V/M/S^2$$

The design amplitude and phase characteristics for the data output channel are plotted as solid curves in Figure 9.4. The measured values taken from three orthogonal components in a test system (seismometer #018) are also plotted in this figure. The measured values depart from the design response to some extent and there is some scatter between components. It is relatively easy, however, to fit the individual transfer function polynomials to the measured data. The departure of measured and design points at periods above 20 seconds is caused by a shortening of the time constant, τ_1, perhaps due to a finite resistive path through the modulator. Two factors affect the closed-loop sensor characteristics that account for the differences below a period of 3 seconds: one is a variation in loop gain, G_1; the other is variation in the motor constants and subsequent differences in the time constant τ_k. By perturbing these three parameters a transfer function to best fit the experimental vertical-component data yields

$$DO(s)\ (018Z) = \frac{K_o\ (s + 47.62)(s + .1621)\ s\ a(s)}{(s + 4.4597 \pm 3.3985j)(s + 38.6)(s + .1514)(s + .1613)(s + 100)(s + 264)}$$

where K_o is a sensitivity constant. The computed and measured data are shown in Figure 9.5. Maximum deviation in amplitude is 1.2% and maximum deviation in phase is 3^o. The fact that a polynomial can be fitted this smoothly to the measured data supports our conclusion that the steady-state measurements taken during special calibration tests described in Section 5.0 are accurate to within 2% in amplitude and 2^o in phase.

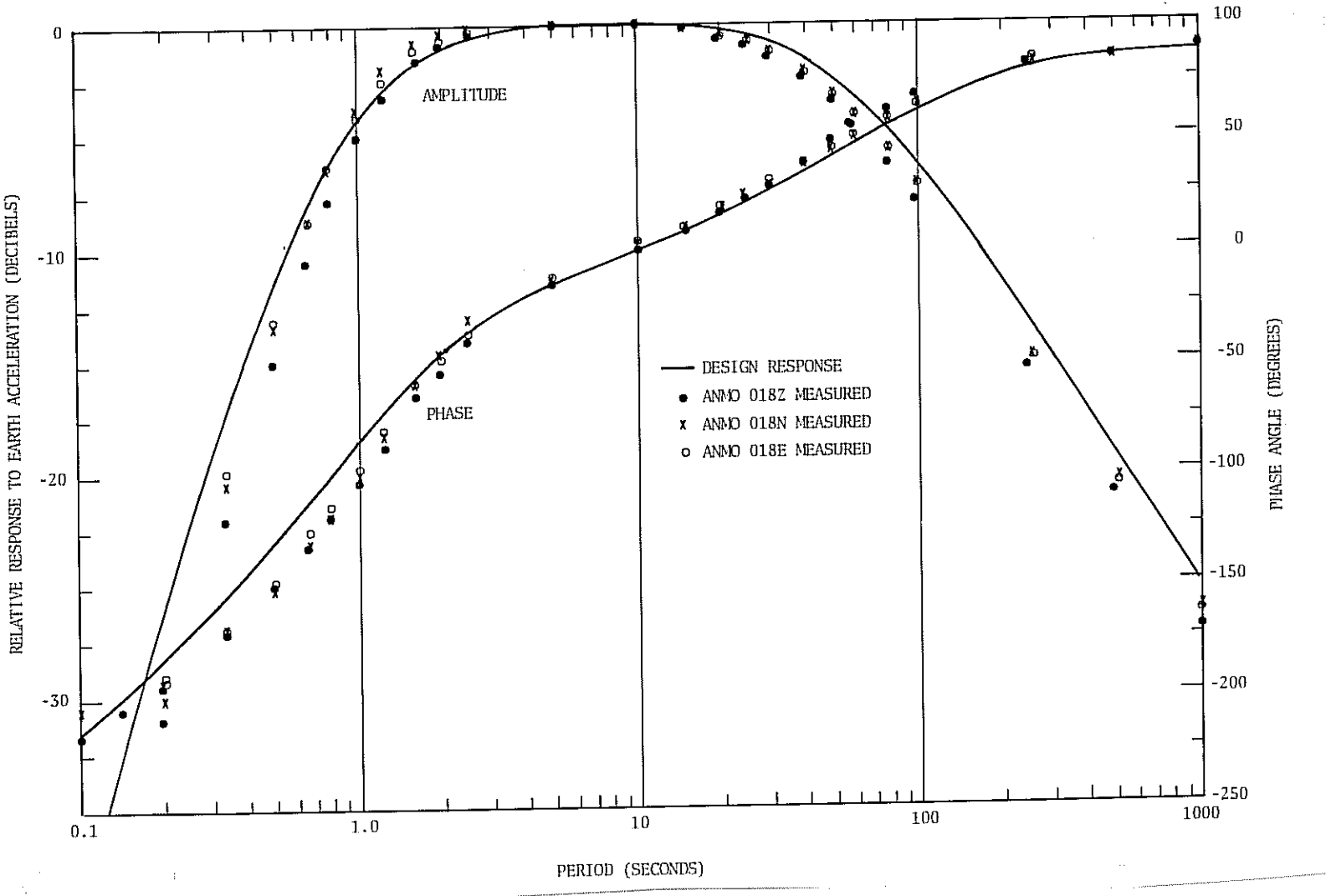

Figure 9.4.--Computed design amplitude and phase characteristics of a data output channel versus measured points taken from three orthogonal components of a test system.

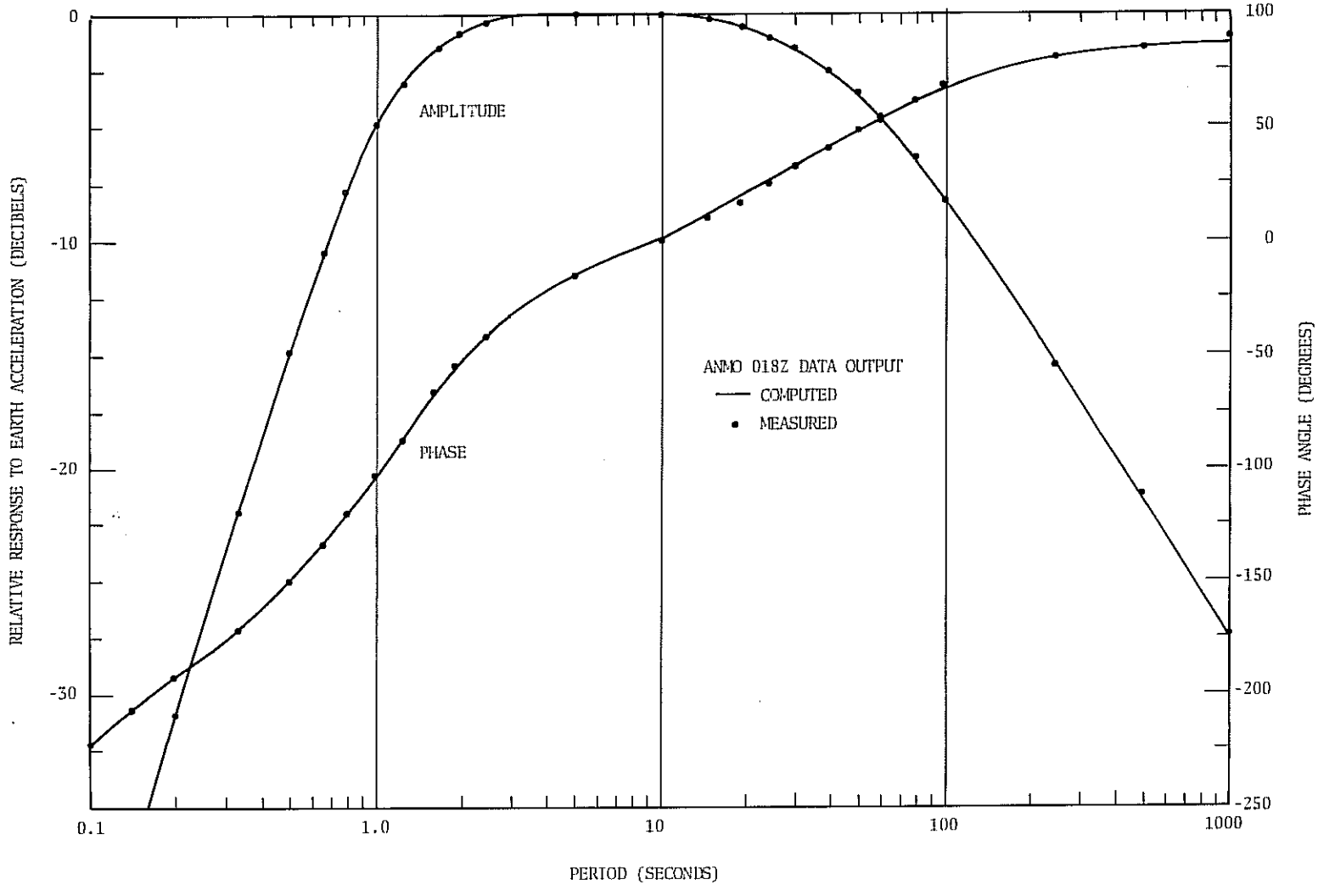

Figure 9.5.--Computed amplitude and phase characteristics fitted to measured points taken from the vertical-component data output channel of the ANMO seismometer.

Precise steady-state measurements of the type just described have been made at the data outputs of only a few of the seismometers to date. Routine station measurements are made at the output of the seismic filters only. In order to derive the nominal transfer characteristics for the SRO system, it has been necessary to average these routine measurements, subtract the seismic filter response, and fit the polynomial to the resulting data. Since the transfer characteristics of the seismic filters are known (they are measured separately), the procedure for deriving the data output nominal response is straightforward and does not require any assumptions. Again, the polynomials have been fitted by perturbing the three designated parameters. Then the nominal relative mass position output is

$$MPO(s)\ (nom) = \frac{(s + .126)(s + 47.6)a(s)}{(s + 4.65 \pm 3.46j)(s + .118)(s + 40.7)(s + 134)}\ V/M/S^2$$

and the nominal relative data output is

$$DO(s)\ (nom) = \frac{(s + .126)(s + 47.6)s\ a(s)}{(s + 4.65 \pm 3.46j)(s + .118)(s + .15)(s + 40.7)(s + 100)(s + 264)}\ V/M/S^2$$

These transfer functions will be modified in the future, if necessary, as the more accurate steady-state measurements are made at the stations.

9.3 Seismic Filters

The two types of seismic filters in the SRO system are used to shape the data output signals into separate short- and long-period bands. The short-period seismic filter has a two-pole low-pass filter section cornered at 2.86 Hz and with a relative damping of 1.0, and a two-pole bandpass filter section with a center frequency at 10 Hz and a relative damping of 1.0. The filter gain is 0.38 at a frequency of 2.5 Hz. According to the manual,

the filter section tolerances for frequency and damping are ± 5%. Measurements made on 14 short-period filters yielded slightly different transfer characteristics than the design response given above. Based on these measurements, the nominal transfer function for this filter is

$$SPF(s) = \frac{(291.4)(4006)s}{(s + 16.73 \pm 3.397j)(s + 63.29)(s + 63.29)}$$

Nominal amplitude and phase characteristics of the short-period filter are plotted in Figure 9.6.

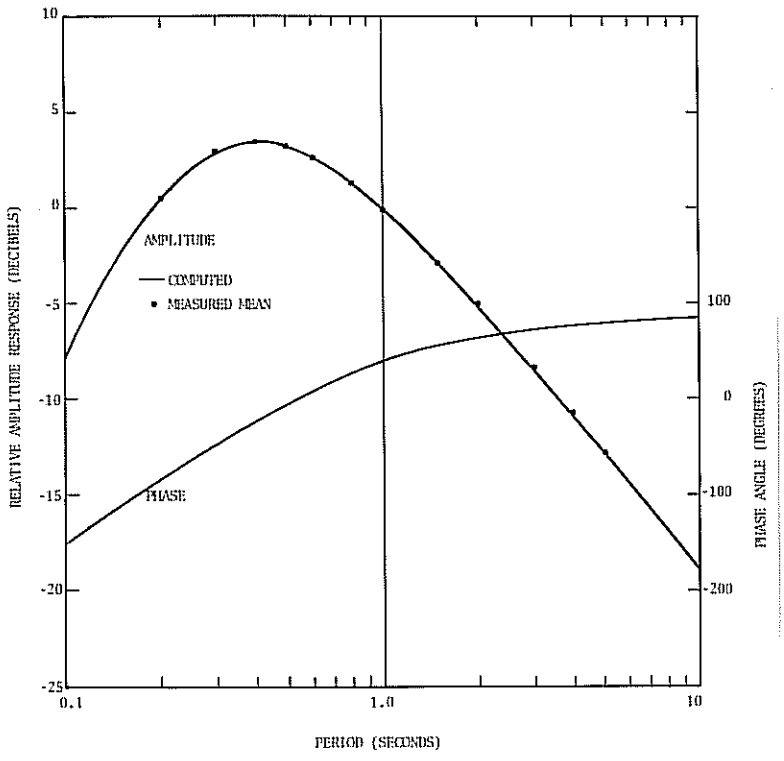

Figure 9.6.--Computed amplitude and phase characteristics of the SRO short-period filter. Measured points on the amplitude curve represent mean values of 14 samples.

The SRO long-period seismic filter has 2 two-pole low-pass filter sections, one with a .0266 Hz corner and 0.8 relative damping and the other with a .050 Hz corner with 0.64 relative damping; 2 single-pole high-pass filters, one with a 0.004 Hz corner and the other with a 0.0015 Hz corner; and a twin-T notch filter with a null at 0.167 Hz. Fortunately, the design response of the long-period filter matches the measured data very closely. The average values of the data points for 45 measurements agree with the computed values to within 2% at all points except at periods between 5 and 7 seconds where rather wild fluctuations can occur because of slight variations in the notch frequency. The nominal (and design) transfer function for the long-period filter is

$$F(s) = \frac{(s \pm 1.053j)}{(s + .2821)\ (s + 3.928)} \quad \frac{(.0987)}{(s + .201 \pm .2415j)} \quad \frac{(.0279)}{(s + .1337 \pm .1001j)} \quad \frac{s}{(s + .02513)} \quad \frac{s}{(s + .00924)}$$

Amplitude and phase characteristics of the long-period filter are plotted in Figure 9.7.

9.4 Anti-Aliasing Filters

Originally, anti-aliasing filters were used in both short- and long-period channels of the SRO system. As we stated earlier, the short-period anti-aliasing filters were removed because of excessive noise and they have not been replaced. Prior to their removal, the manufacturer of the SRO recording system attempted to reduce the filter noise by installing single-pole, 16 Hz, low-pass sections between the filters and the analog-to-digital converters. The low-pass sections have since been removed (see Table 2.1). They had very little effect on the system response at frequencies below 5 Hz, but for accuracy they are included in the system transfer functions where appropriate. The transfer function of the low-pass section is

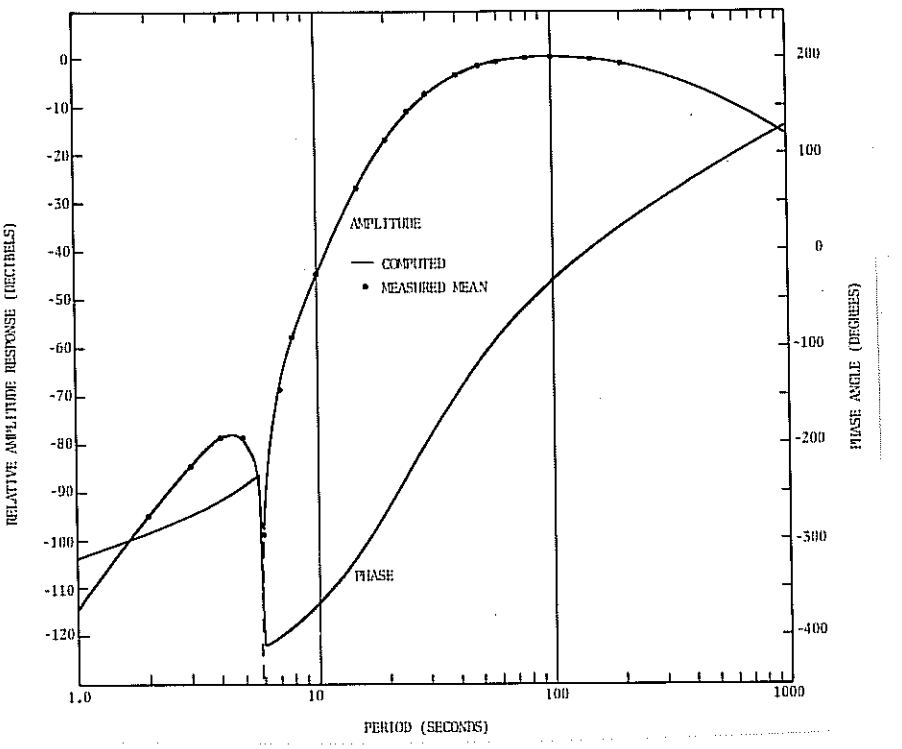

Figure 9.7.--Computed amplitude and phase characteristics of the SRO long-period filter. Measured points on amplitude curve represent mean values of 45 samples.

$$LPS(s) = 100/(s + 100)$$

As originally configured, the long-period anti-aliasing filters used in the SRO systems had four-pole Butterworth responses. Because of difficulty in adjusting and maintaining the DC offset in these filters (and some noise problems as well), they have been replaced with four-pole Bessel-response filters. The date of the change at each station is given in Table 2.1. Both types of filters have a substantial effect on the long-period amplitude response at periods below 15 seconds and on the long-period phase response at periods below 100 seconds. The transfer characteristics of these filters vary from tabular four-pole Butterworth and Bessel responses. This is especially true of the Butterworth filter as illustrated in Figure 9.8,

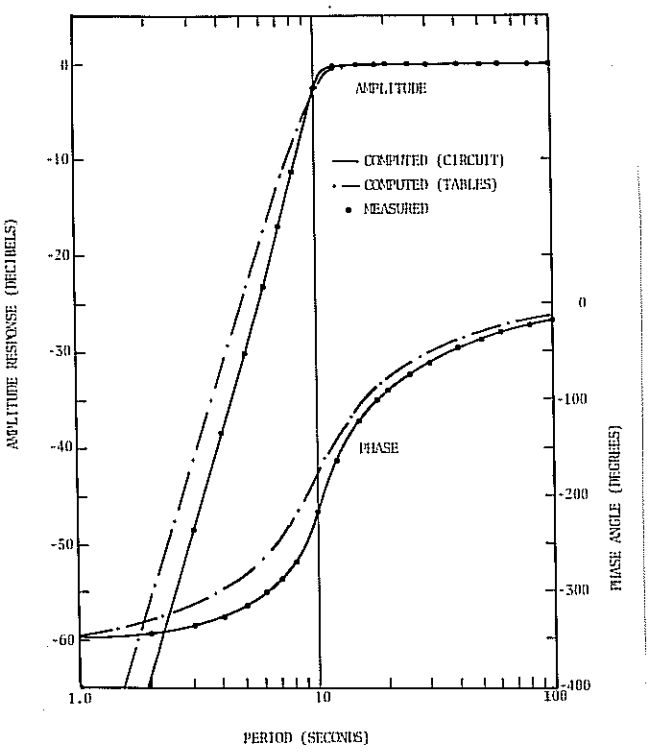

Figure 9.8.--Amplitude and phase characteristics of Butterworth anti-aliasing filter. Solid line was derived from circuit analysis, broken line from tables; points were measured on test unit.

which compares the design response, computed response based on actual circuit values, and measured response. The Butterworth transfer function, derived from circuit analysis, is

$$AAFI(s) = \frac{.0607}{(s + .3334 \pm .2358j)(s + .1378 \pm .5873j)}$$

The Bessel filter transfer function, also derived from circuit analysis, is

$$AAF\ II(s) = \frac{.6050}{(s + .8547 \pm .2555j)(s + .5415 \pm .6834j)}$$

The amplitude and phase characteristics of the Bessel filters are shown

in Figure 9.9.

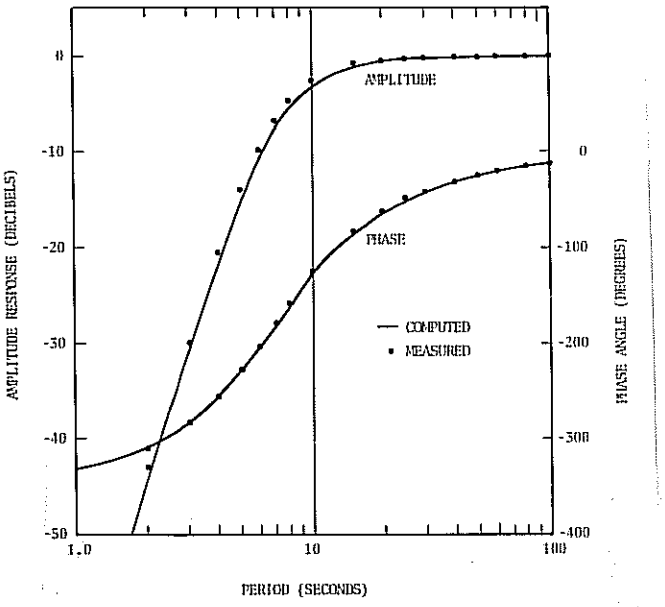

Figure 9.9.--Amplitude and phase response characteristics of Bessel anti-aliasing filter. Solid line was derived from circuit analysis; points were measured on test system.

9.5 Nominal System Transfer Functions

System transfer functions are obtained by taking the product of the appropriate elemental transfer functions. The results are summarized in Table 9.1 for all the current and past operating configurations of the SRO systems. Recall that the terminology is defined in Figure 9.1. Note that the nominal transfer functions are given with respect to an input of earth displacement, x(s), rather than earth acceleration. Impulse responses derived from the nominal transfer functions are shown in Figures 9.10 through 9.13.

----------SPA(s)/SPD(s)-----

Poles	Zeros
s + 4.648 ± 3.463j	s^2
s + .1179	s + .1243
s + 40.73	s + 47.62
s + 100	
s + .1500	s
s + 264	
s + 16.73 ± 3.397j	
s + 63.29	s
s + 63.29	

K_o = 7.135 x 10^9

----------SPDF(s)---------

Poles	Zeros
s + 4.648 ± 3.463j	s^2
s + .1179	s + .1243
s + 40.73	s + 47.62
s + 100	
s + .1500	s
s + 264	
s + 16.73 ± 3.397j	
s + 63.29	s
s + 63.29	
s + 100	

K_o = 7.148 x 10^{11}

----------SSPA(s)/SSPD(s)----

Poles	Zeros
s + 4.648 ± 3.463j	s^2
s + .1179	s + .1243
s + 40.73	s + 47.62
s + 134	
s + 16.73 ± 3.397j	
s + 63.29	s
s + 63.29	

K_o = 3.616 x 10^7

----------SSPDF(s)--------

Poles	Zeros
s + 4.648 ± 3.463j	s^2
s + .1179	s + .1243
s + 40.73	s + 47.62
s + 134	
s + 16.73 ± 3.397j	
s + 63.29	s
s + 63.29	
s + 100	

K_o = 3.623 x 10^9

----------LPA(s)---------

Poles	Zeros
s + 4.648 ± 3.463j	s^2
s + .1179	s + .1243
s + 40.73	s + 47.62
s + 100	
s + .1500	s
s + 264	
s + 3.928	s ± 1.053j
s + .2820	
s + .2010 ± .2410j	
s + .1337 ± .1001j	
s + .0251	s
s + .00924	s

K_o = 1.609 x 10^5

----------LPD I(s)--------

Poles	Zeros
s + 4.648 ± 3.463j	s^2
s + .1179	s + .1243
s + 40.73	s + 47.62
s + 100	
s + .1500	s
s + 264	
s + 3.928	s ± 1.053j
s + .2820	
s + .2010 ± .2410j	
s + .1337 ± .1001j	
s + .0251	s
s + .00924	s
s + .3334 ± .2358j	
s + .1378 ± .5873j	

K_o = 9.785 x 10^3

----------LPD II(s)--------

Poles	Zeros
s + 4.648 ± 3.463j	s^2
s + .1179	s + .1243
s + 40.73	s + 47.62
s + 100	
s + .1500	s
s + 264	
s + 3.928	s ± 1.053j
s + .2820	
s + .2010 ± .2410j	
s + .1337 ± .1001j	
s + .0251	s
s + .00924	s
s + .8547 ± .2555j	
s + .5415 ± .6834j	

K_o = 1.023 x 10^5

----------MPO(s)---------

Poles	Zeros
s + 4.648 ± 3.463j	s^2
s + .1179	s + .1243
s + 40.73	s + 47.62
s + 134	

K_o = normalizing factor at period of 1 second (SP) or 25 seconds (LP)

October 1979

Table 9.1.-- Summary of nominal SRO transfer functions.

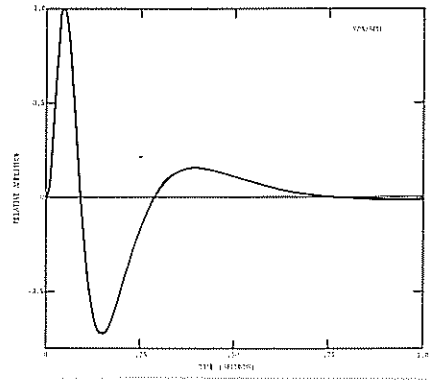

Figure 9.10.--Time response of SRO short-period channel to an impulse of displacement.

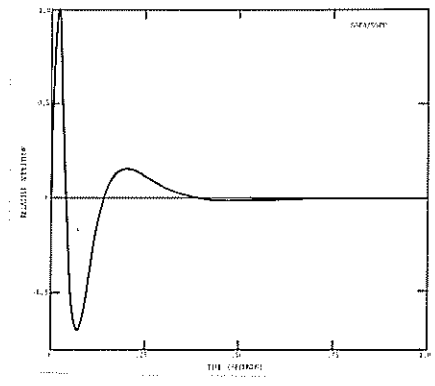

Figure 9.11.--Time response of SRO special short-period channel to an impulse of displacement.

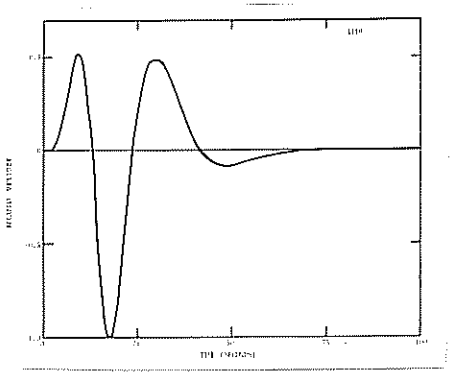

Figure 9.12.--Time response of SRO long-period channel (Butterworth anti-aliasing filter) to an impulse of displacement.

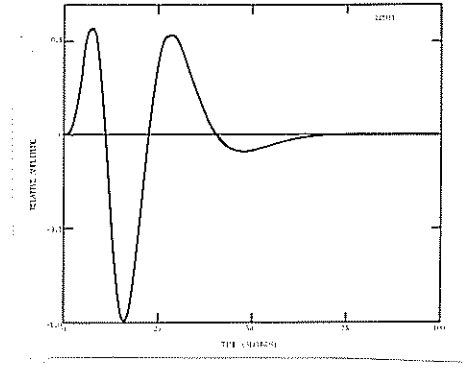

Figure 9.13.--Time response of SRO long-period channel (Bessel anti-aliasing filter) to an impulse of displacement.

9.6 SRO Component Transfer Functions

As indicated on several previous occasions in this report, special calibration tests are currently being made on the SRO system; this testing results in individual transfer functions tailored for each component. The tests involve the determination of steady-state phase and amplitude reponse of the data output and mass position channels of each seismometer component, each seismic filter, and each anti-aliasing filter. The individual transfer functions are then obtained by fitting the polynomials to the measured data in a least squares sense. To date these tests have been completed on only the Albuquerque SRO system. Data from other stations will become available in the future.

The transfer functions derived for the four Albuquerque SRO channels are given in Table 9.2. Tabular values computed from these transfer functions are compared with measured values in Table 9.3. Clearly, both measurement errors and analytical errors in deriving the transfer functions are very small.

SPZ		LPZ		LPN		LPE	
Poles	Zeros	Poles	Zeros	Poles	Zeros	Poles	Zeros
s + 4.460 ± 3.399j	s^2	s + 4.460 ± 3.399j	s^2	s + 4.242 ± 4.154j	s^2	s + 5.002 ± 3.822j	s^2
s + .1514	s + .1621	s + .1514	s + .1621	s + .1516	s + .1399	s + .1540	s + .1415
s + 38.57	s + 47.62	s + 38.57	s + 47.62	s + 38.57	s + 47.62	s + 38.57	s + 47.62
s + 100		s + 100		s + 100		s + 100	
s + .1613	s	s + .1613	s	s + .1389	s	s + .1408	s
s + 264		s + 264		s + 264		s + 264	
s + 16.86 ± 3.423j		s + 3.928	s ± 1.053j	s + 3.928	s ± 1.053j	s + 3.928	s ± 1.053j
s + 63.29	s	s + .2820		s + .2820		s + .2820	
s + 63.29		s + .2010 ± .2410j		s + .2010 ± .2410j		s + .2010 ± .2410j	
		s + .1337 ± .1001j		s + .1337 ± .1001j		s + .1337 ± .1001j	
		s + .0251	s	s + .0246	s	s + .0251	s
		s + .00924	s	s + .00924	s	s + .00924	s
		s + .8547 ± .2555j		s + 1.007 ± .3072j		s + .8974 ± .2738j	
		s + .5415 ± .6834j		s + .6390 ± .8064j		s + .5686 ± .7176j	
$K_o = 6.614 \times 10^9$		$K_o = 9.160 \times 10^4$		$K_o = 1.920 \times 10^5$		$K_o = 1.322 \times 10^5$	

October 1979

Table 9.2.--ANMO transfer functions for digital records only.

SPZ

PERIOD (seconds)	COMPUTED amplitude (relative)	COMPUTED phase angle (deg.)	MEASURED* amplitude (relative)	MEASURED* phase angle (deg.)	DIFFERENCE %	DIFFERENCE deg.
10.000	.00199	267	.00207	265	3.8	2
5.000	.0160	244	.0164	244	2.3	0
2.500	.120	208	.120	207	0.0	1
2.000	.221	191	.221	191	0.0	0
1.670	.350	174	.351	174	0.2	0
1.250	.671	143	.672	143	0.1	0
1.000	1.00	116	1.00	116	0.0	0
.833	1.29	92	1.29	91	0.0	1
.667	1.61	65	1.61	63	0.0	0
.500	1.91	25	1.89	25	0.8	0
.333	1.93	-30	1.94	-30	0.2	0
.250	1.66	-69	1.68	-68	1.3	1
.200	1.34	-99	1.32	-99	1.4	0
.143	.837	-145	.843	-145	0.7	0

*corrected for calibration circuit

LPZ

PERIOD (seconds)	COMPUTED amplitude (relative)	COMPUTED phase angle (deg.)	MEASURED amplitude (relative)	MEASURED phase angle (deg.)	DIFFERENCE %	DIFFERENCE deg.
1022	.0000167	393	.0000165	392	0.7	1
516	.000340	352	.000342	351	0.6	1
258	.00501	298	.00509	296	1.6	2
99.0	.110	199	.109	199	0.3	0
78.4	.207	167	.208	167	0.4	0
59.6	.402	123	.405	122	0.7	1
50.1	.571	91	.573	90	0.4	1
39.7	.818	42	.823	42	0.6	0
30.1	1.01	-23	1.02	-24	0.5	1
25.0	1.00	-71	1.00	-72	0.0	1
20.0	.808	-131	.801	-132	0.8	1
14.5	.396	-218	.392	-218	1.1	0
9.8	.0886	-321	.0883	-319	0.2	2
7.9	.0249	-377	.0254	-378	1.7	1

LPN

PERIOD (seconds)	COMPUTED amplitude (relative)	COMPUTED phase angle (deg.)	MEASURED amplitude (relative)	MEASURED phase angle (deg.)	DIFFERENCE %	DIFFERENCE deg.
1011	.0000196	392	.0000198	390	1.2	2
514	.000385	351	.000388	348	0.8	3
258	.00553	296	.00555	294	0.4	2
99.2	.117	198	.116	198	1.2	0
79.6	.212	168	.210	168	1.0	0
59.6	.421	122	.419	122	0.5	0
50.0	.593	90	.593	90	0.0	0
39.9	.829	44	.826	45	0.4	0
30.1	1.02	-20	1.02	-19	0.0	1
24.9	.988	-67	1.00	-67	0.2	0
20.0	.807	-124	.803	-123	0.5	1
14.4	.395	-207	.399	-205	1.0	2
9.9	.102	-298	.102	-296	0.0	2
7.8	.0286	-354	.0281	-352	1.	2

LPE

PERIOD (seconds)	COMPUTED amplitude (relative)	COMPUTED phase angle (deg.)	MEASURED amplitude (relative)	MEASURED phase angle (deg.)	DIFFERENCE %	DIFFERENCE deg.
1006	.0000196	392	.0000199	391	1.7	1
502	.000416	350	.000412	349	0.9	1
251	.00601	294	.00599	293	0.3	1
100.4	.113	199	.112	198	0.5	1
79.9	.209	168	.206	167	1.6	1
59.8	.417	122	.415	122	0.6	0
48.2	.633	82	.636	85	0.5	3
40.0	.828	42	.834	42	0.7	0
30.1	1.02	-25	1.03	-25	1.0	0
25.0	1.00	-71	1.00	-73	0.0	2
20.0	.803	-131	.807	-131	0.5	0
15.0	.434	-207	.436	-209	0.5	2
10.0	.0993	-310	.100	-312	0.7	2
8.0	.0286	-366	.0284	-364	0.4	2

Table 9.3.--ANMO transfer functions vs. measured data.

ACKNOWLEDGEMENT

This work was supported in part by the Defense Advanced Research Projects Agency. We wish to thank Ray Buland of the U.S. Geological Survey and Howard (Jim) Durham of Sandia Laboratories for reviewing the manuscript and providing many helpful suggestions.

REFERENCES

Bendat, J.S. and A.G. Piersol (1971). Random Data: Analysis and Measurement Procedures, John Wiley & Sons, New York.

Berger, J., D.C. Agnew, R.L. Parker, and W.E. Farrell (1979). Seismic system calibration: 2. cross-spectral calibration using random binary signals, Bull. Seism. Soc. Am. 69, 271-288.

Brune, J.N. and J. Oliver (1959). The seismic noise of the earth's surface, Bull. Seism. Soc. Am. 49, 349-353.

Ensco, Inc. (1975). Non-linear effects in seismometers, Final Technical Report, Ensco, Inc., Springfield, Virginia.

Farrell, W.E. and J. Berger (1979). Seismic system calibration: 1. parametric models, Bull. Seism. Soc. Am. 69, 251-270.

Hanks, T.C. and M. Wyss (1972). The use of body-wave spectra in the determination of seismic source parameters, Bull. Seism. Soc. Am. 62, 561-589.

Holcomb, L.G. (1975). Borehole evaluation of the Teledyne-Geotech 36000 seismometer system at Albuquerque, New Mexico, February-June 1974, U.S. Geol. Survey Open-File Report 75-373.

McCowan, D.W. and R.T. Lacoss (1978). Transfer functions for the seismic research observatory seismograph system, Bull. Seism. Soc. Am. 68, 501-512.

Otnes, R.K. and L. Enochson (1972). Digital Time Series Analysis, John Wiley & Sons, New York.

Peterson, J., H.M. Butler, L.G. Holcomb, and C.R. Hutt (1976). The seismic research observatory, Bull. Seism. Soc. Am. 66, 2049-2068.

Phoenix Data (1973). Operation and maintenance manual: 8000 series ADC subsystem, model 8012-2361. Phoenix Data, Inc., Phoenix, Arizona.

Sherwin, J.R. and G.C. Kraus (1974). Final Report, Project T/3703. Teledyne-Geotech Technical Report 73-19.

Stearns, S.D. (1975). Digital Signal Analysis, Hayden Book Company, Rochelle Park, New Jersey.

Teledyne-Geotech (1976a). Operation and maintenance manual: USGS sensor system M38600. Teledyne-Geotech, Inc., Garland, Texas.

Teledyne-Geotech (1976b). Operation and maintenance manual: borehole seismometer system M36000, part I. Teledyne-Geotech, Inc., Garland, Texas.

Teledyne-Geotech (1976c). Operation and maintenance manual: borehole seismometer system M36000, part II (schematics). Teledyne-Geotech Inc., Garland, Texas.

Teledyne-Geotech (1976d). Operation and maintenance manual: test set/ controller M37960. Teledyne-Geotech Inc., Garland, Texas.

Teledyne-Geotech (1976e). Operation and maintenance manual: long-period filter M38840. Teledyne-Geotech Inc., Garland, Texas.

Teledyne-Geotech (1976f). Operation and maintenance manual: short-period filter M38850. Teledyne-Geotech, Inc., Garland, Texas.

Teledyne-Geotech (1976g). Operation and maintenance manual: calibrator M38750. Teledyne-Geotech, Inc., Garland, Texas.
Teledyne-Geotech (1976h). Operation and maintenance manual: winch M38760. Teledyne-Geotech, Inc., Garland, Texas.
Teledyne-Geotech (1976i). Operation and maintenance manual: portable power supply M38630. Teledyne-Geotech, Inc., Garland, Texas.
Unitech (1974). Operation and maintenance manual: seismic research observatory data recording system. Unitech, Inc., Austin, Texas.